Opto-Electronic Science

CN 51-1800/O4 ISSN 2097-0382 (Print) ISSN 2097-4000 (Online)

Control of light–matter interactions in two-dimensional materials with nanoparticle-on-mirror structures

Shasha Li, Yini Fang and Jianfang Wang

Citation: Li SS, Fang YN, Wang JF. Control of light–matter interactions in two-dimensional materials with nanoparticle-on-mirror structures. *Opto-Electron Sci* **3**, 240011 (2024).

https://doi.org/10.29026/oes.2024.240011

Received: 18 March 2024; Accepted: 13 May 2024; Published online: 28 June 2024

Related articles

Highly enhanced UV absorption and light emission of monolayer WS_2 through hybridization with Ti_2N MXene quantum dots and g-C_3N_4 quantum dots

Anir S. Sharbirin, Rebekah E. Kong, Wendy B. Mato, Trang Thu Tran, Eunji Lee, Jolene W. P. Khor, Afrizal L. Fadli, Jeongyong Kim

Opto-Electronic Advances 2024 **7**, 240029 doi: 10.29026/oea.2024.240029

2D Nb_2CT_x MXene/MoS_2 heterostructure construction for nonlinear optical absorption modulation

Yiduo Wang, Yingwei Wang, Yulan Dong, Li Zhou, Jianlong Kang, Ning Wang, Yejun Li, Xiaoming Yuan, Zhengwei Zhang, Han Huang, Mengqiu Long, Si Xiao, Jun He

Opto-Electronic Advances 2023 **6**, 220162 doi: 10.29026/oea.2023.220162

Perovskite-transition metal dichalcogenides heterostructures: recent advances and future perspectives

Ahmed Elbanna, Ksenia Chaykun, Yulia Lekina, Yuanda Liu, Benny Febriansyah, Shuzhou Li, Jisheng Pan, Ze Xiang Shen, Jinghua Teng

Opto-Electronic Science 2022 **1**, 220006 doi: 10.29026/oes.2022.220006

Active tuning of anisotropic phonon polaritons in natural van der Waals crystals with negative permittivity substrates and its application in energy transport

Shuo Chen, Xiaohu Wu, Ceji Fu

Opto-Electronic Science 2024 **3**, 240002 doi: 10.29026/oes.2024.240002

More related article in Opto-Electronic Journals Group website

OES Opto-Electronic Science

http://www.oejournal.org/oes

OE_Journal

Website

Opto-Electronic Science

Review

July 2024, Vol. 3, No. 7

DOI: 10.29026/oes.2024.240011

Control of light–matter interactions in two-dimensional materials with nanoparticle-on-mirror structures

Shasha Li[1], Yini Fang[2] and Jianfang Wang[2]*

Light–matter interactions in two-dimensional (2D) materials have been the focus of research since the discovery of graphene. The light–matter interaction length in 2D materials is, however, much shorter than that in bulk materials owing to the atomic nature of 2D materials. Plasmonic nanostructures are usually integrated with 2D materials to enhance the light–matter interactions, offering great opportunities for both fundamental research and technological applications. Nanoparticle-on-mirror (NPoM) structures with extremely confined optical fields are highly desired in this aspect. In addition, 2D materials provide a good platform for the study of plasmonic fields with subnanometer resolution and quantum plasmonics down to the characteristic length scale of a single atom. A focused and up-to-date review article is highly desired for a timely summary of the progress in this rapidly growing field and to encourage more research efforts in this direction. In this review, we will first introduce the basic concepts of plasmonic modes in NPoM structures. Interactions between plasmons and quasi-particles in 2D materials, e.g., excitons and phonons, from weak to strong coupling and potential applications will then be described in detail. Related phenomena in subnanometer metallic gaps separated by 2D materials, such as quantum tunneling, will also be touched. We will finally discuss phenomena and physical processes that have not been understood clearly and provide an outlook for future research. We believe that the hybrid systems of 2D materials and NPoM structures will be a promising research field in the future.

Keywords: light–matter interactions; nanoparticle-on-mirror structures; plasmonic enhancement; two-dimensional materials

Li SS, Fang YN, Wang JF. Control of light–matter interactions in two-dimensional materials with nanoparticle-on-mirror structures. *Opto-Electron Sci* **3**, 240011 (2024).

Introduction

Two-dimensional (2D) materials are a promising solution for next-generation electronic and optoelectronic devices. The most investigated 2D materials range from semimetallic graphene, semiconducting transition metal dichalcogenides (TMDCs) and black phosphorus, to insulating hexagonal boron nitride (h-BN). 2D materials show significant advantages for the construction of optoelectronic and photonic devices. First, their optical responses cover a wide electromagnetic spectrum from ultraviolet to terahertz frequencies[1]. Second, 2D materials possess intriguing optical properties. For example, graphene can support intrinsic plasmons that are tunable and adjustable, which promises new applications for conventional plasmonics[2]. TMDC monolayers show valley pseudospins owing to broken spatial inversion symmetry, offering a new degree of freedom for information

[1]School of Integrated Circuits, Sun Yat-sen University, Shenzhen 518107, China; [2]Department of Physics, The Chinese University of Hong Kong, Shatin, Hong Kong SAR 999077, China.

*Correspondence: JF Wang, E-mail: jfwang@phy.cuhk.edu.hk

Received: 18 March 2024; Accepted: 13 May 2024; Published online: 28 June 2024

storage and processing[3,4]. Black phosphorus possesses strong intrinsic in-plane anisotropy, which is promising for the realization of novel thin-film infrared polarizers and polarization-related sensors[5]. Hyperbolic phonon polaritons in h-BN have aroused intense interest in near-field optical imaging, guiding, and focusing applications[6]. Third, layer-by-layer stacking is allowed for 2D materials, without the lattice mismatch problem[7]. Van der Waals stacking enables multi-functionality and innovative device engineering for spintronics and opto-spintronics[8]. Therefore, light–matter interactions in 2D materials have become the research focus in the past decades.

Localized surface plasmon resonance (LSPR) arises from the collective oscillations of free charge carriers in bounded geometries like metallic particles and voids at the sub-wavelength scale. LSPR has been well known for synthetically controllable plasmon resonance wavelengths, large scattering/absorption cross-sections, and high electromagnetic field enhancement. It has been exploited as a powerful tool for enhancing light–matter interactions[9]. In the past decade, plasmonic nanostructures have been integrated with 2D materials for a range of applications such as solar energy harvesting[10], sensing[11], optics/optoelectronics[12], and quantum nanophotonics[13]. In addition to commonly used individual plasmonic nanoparticles, plasmonic hybrid structures consisting of closely spaced metal nanoparticles are highly desired for the plasmonic modulation of 2D materials. The nanogaps in such plasmonic hybrid structures, such as plasmonic dimers, give rise to coupled plasmon resonances and "hot-spots" with higher local field enhancement and smaller mode volumes[14]. 2D materials embedded into plasmonic dimers can feel the strongly confined optical fields, which results in improved photoresponse[15]. However, it is generally difficult to place a 2D material inside the nanogap of a plasmonic dimer. The surface adatoms, cracks, and strain, which are unintentionally introduced during the preparation process, will cause degradation to the optical properties of 2D materials. Nanoparticle-on-mirror (NPoM) structures, which are another type of plasmonic hybrid structures supporting strongly confined optical fields, can be an elegant solution for the integration with 2D materials. The NPoM structure is made of a plasmonic nanoparticle on a smooth metal film with a nanospacer in between. The NPoM structure can confine optical fields with surprisingly low loss and with volumes below 1 cubic nanometers[16], which is challenging to achieve with single nanoparticles. 2D materials are well-suited for integration into NPoM structures, forming subnanometer gaps[17]. The excitons in the gap region are coupled with the strong plasmon resonance, which can be tailored across weak to strong coupling regimes[18]. The ultraconfined plasmonic field can also lead to nonlinear optical effects[19]. In addition, the atomic nature of 2D materials pushes conventional plasmonics into the quantum regime[20]. The integration of plasmonic NPoM structures with 2D materials is of great interest to both fundamental research and promising applications.

In this review, we highlight the research advances in the coupling between 2D materials and NPoM structures. We will start with a brief introduction to the plasmon resonances in NPoM structures as well as the preparation of 2D material-embedded NPoM structures. The imperfect factors that affect the optical properties of the hybrid structures will be discussed. We will then introduce the light–matter interactions in the hybrid system, with emphasis on the plasmon–exciton coupling. The possible quantum tunneling occurring in the subnanometer gap will be discussed. The potential applications will also be presented. We will finally point out unanswered questions and provide an outlook for future studies.

Plasmon resonances in NPoM structures

NPoM structures are composed of plasmonic nanoparticles deposited on mirror substrates made of Au or Ag, with a thin dielectric gap layer in between. Such structures exhibit strong confinement of optical fields, resulting in localized optical responses at the nanogap. To understand the optical confinement in such plasmonic nanocavities intuitively, the finite-difference time-domain (FDTD) simulation results of a nanosphere-on-mirror (NSoM) structure are provided (Fig. 1). In the simulation, a 100 nm Au nanosphere (NS) is positioned on a Au film, separated by a 1 nm dielectric spacer. Such a spacer thickness is suitable for monolayer 2D materials. The Au NS is taken as an ideal sphere, with point contact on the substrate. The system is illuminated by a plane wave with wavevector $\boldsymbol{k}$ either parallel (Fig. 1(a)) or perpendicular (Fig. 1(c)) to the mirror plane, corresponding to the out-of-plane and in-plane excitation, respectively. The simulated scattering cross-sections show pronounced peaks around the wavelength range of 500–1000 nm in both cases. The near-field maps in Fig.

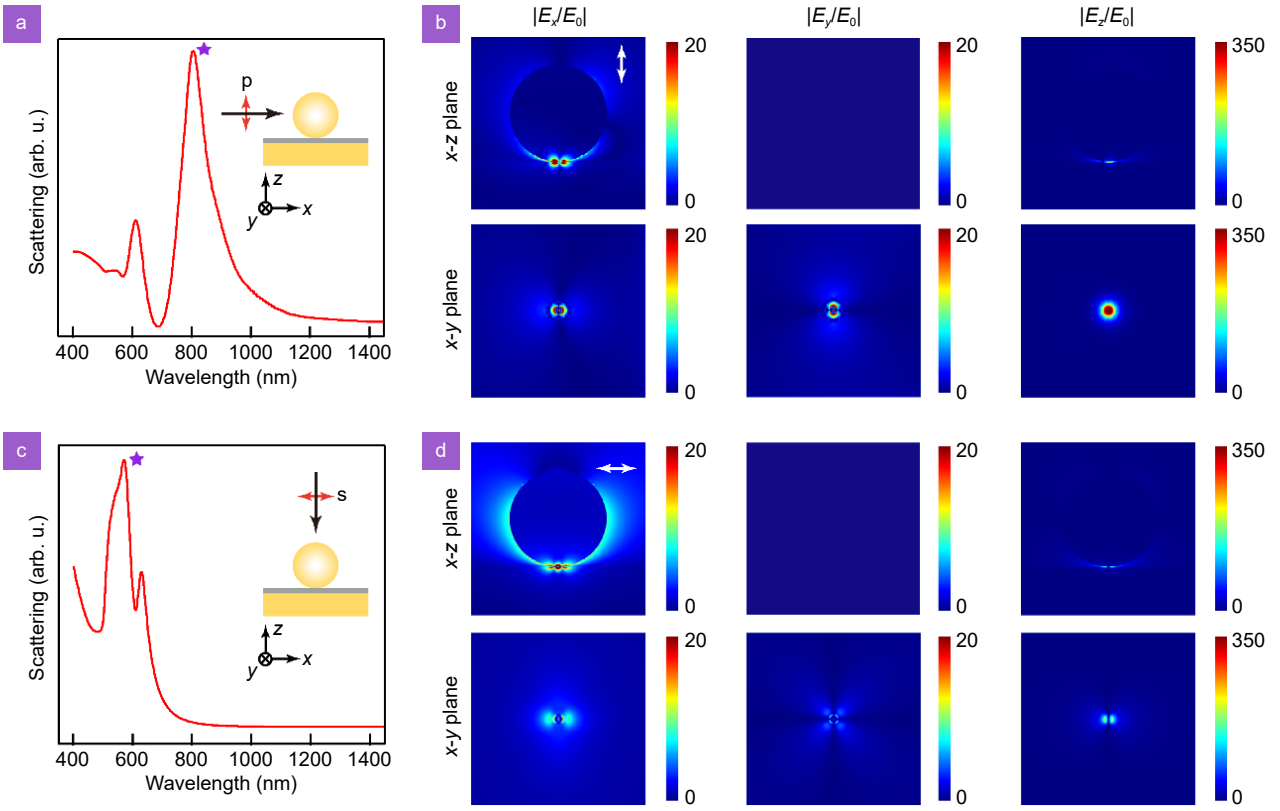

Fig. 1 | Highly confined electromagnetic field in the nanogap. (**a**) Simulated scattering cross-sections of a Au NSoM structure. The schematic of the structure is given in the inset. The diameter of the Au NS is 100 nm. The refractive index of the spacer is taken as a constant (1.45) for simplicity. The thickness is 1 nm. The propagating direction of the excitation light is set to be parallel to the substrate. (**b**) Contours of the electric field intensity enhancement along the different axes at the resonance wavelength marked by the star in (a). (**c**) Simulated scattering cross-sections with an in-plane excitation, where the propagating direction of the excitation light is perpendicular to the substrate. (**d**) Corresponding electric field intensity enhancement at the resonance wavelength marked by the star in (c).

1(b) and 1(d) have two notable features. First, the electromagnetic field is highly confined in the gap region. Second, the out-of-plane field enhancement is significantly larger than the in-plane field enhancement for both excitation conditions. In addition, the field enhancement is much larger under the out-of-plane excitation condition. We will further look into the plasmon modes that generate substantial field enhancement.

The plasmon resonances in an ideal NSoM structure are dominated by the radiative antenna modes (l_n)[21]. The dipolar antenna mode (l_1) is pronounced. As the gap distance is reduced, higher-order antenna modes ($n > 1$) are also efficiently excited. When a circular facet is introduced at the nanosphere base (Fig. 2(a)), which is closer to the experimental situation, gap modes emerge. The resonance modes in the gap are derived from an infinite planar metal-insulator-metal (MIM) model[22]. The finite gap nature is considered by use of a two-dimensional Fabry–Pérot resonator model, which describes the partial reflection of plasmons at the edge of the bottom facet of the NS. For a facet width of w, the resonance wavelengths are given analytically by[22,23]

$$\lambda_i^s \simeq \lambda_p \sqrt{\frac{w\varepsilon_g}{d\alpha_i} + \varepsilon_\infty}\ , \tag{1}$$

where α_i are the zeros of the Bessel functions of the first kind; ε_∞ is the dielectric background; λ_p is the plasma wavelength of gold; d is the gap distance; and ε_g is the dielectric constant of the gap layer. The above equation defines the gap modes s_{mn}, where the indices m and n indicate the number of nodes in the azimuthal and radial directions. These gap modes are dependent on the facet width, spanning a range from the visible to near-infrared region (Fig. 2(b)). The gap modes can be categorized as weakly radiative (solid lines in Fig. 2(b)) or non-radiative (dashed lines in Fig. 2(b)), showing distinct mode symmetries and charge distributions[21]. Their interactions with the antenna modes are therefore completely different. For example, the s_{1n} modes (azimuthal number $m = 1$) exhibit a transverse dipolar nature and swap

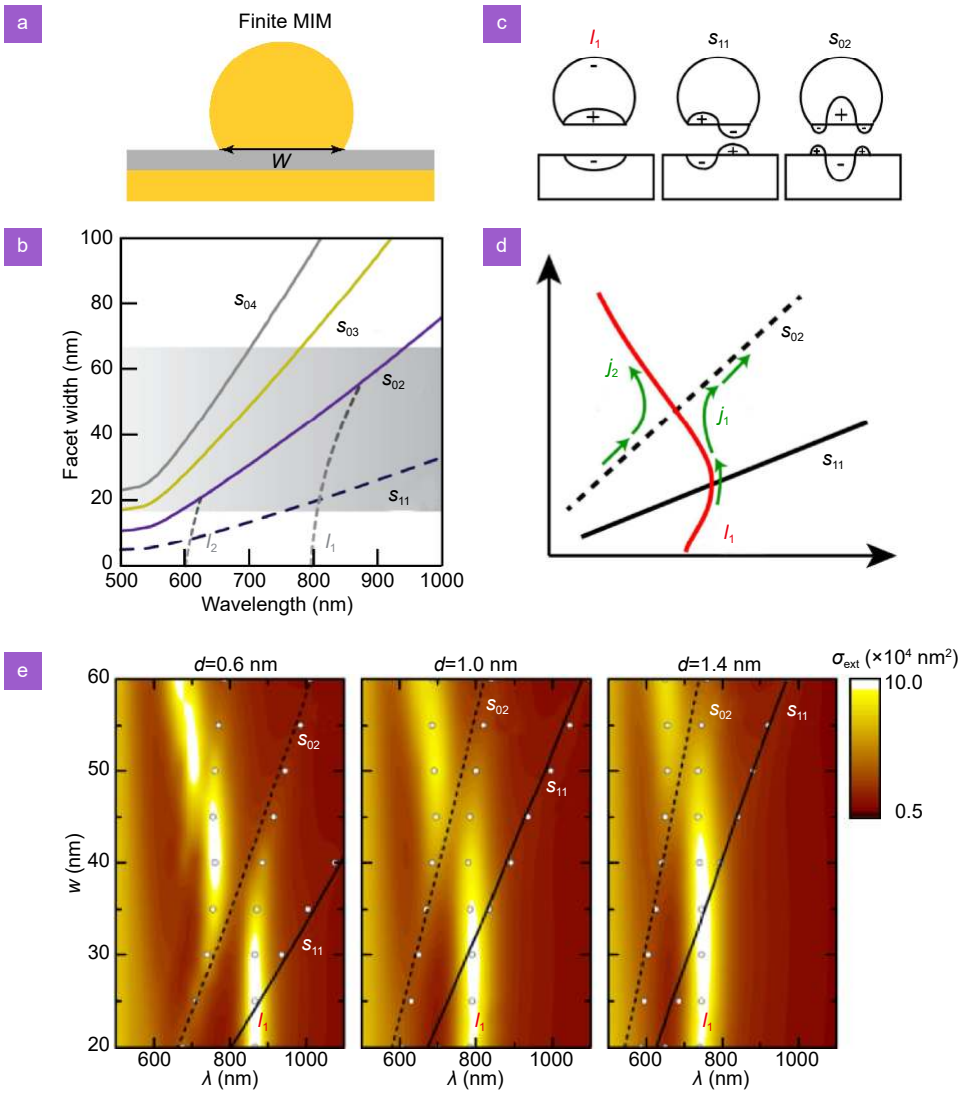

Fig. 2 | Plasmon modes in the nanogap. (**a**) Schematic of a flat-junction NPoM configuration, with a facet width of *w*. (**b**) Antenna modes l_n and gap modes s_{mn} in the NPoM structure, which can be adjusted with the facet width *w*. The shaded area shows an experimentally accessed facet range. (**c**) Charge distributions for the l_1, s_{11}, and s_{02} modes. (**d**) Schematic showing the interactions between the antenna and gap modes. The plasmon modes in the nanogap are the hybridization (j_n) of the antenna and gap modes. (**e**) Extinction cross-sections of a faceted spherical gold nanoparticle in the NPoM structure. The diameter is 80 nm and the spacer thickness is varied from 0.6 to 1.4 nm. Figure reproduced with permission from: (b) ref.[23], Copyright 2014 American Chemical Society; (c–e) ref.[21], Copyright 2015 American Physical Society.

the surface charge sign at each end of the gap (Fig. 2(c)). These modes do not couple to the antenna modes (l_n), which are radially symmetric. In contrast, the s_{0n} modes (azimuthal number m = 0) have the same symmetry as the antenna modes (Fig. 2(c)). They interact and form radiative hybrid modes (j_n). For instance, the l_1 mode meets spectrally with the s_{02} mode, giving rise to the mode anticrossing feature with two hybridized modes j_1 and j_2 (Fig. 2(d)). The antenna modes depend on the nanoparticle size, facet width, and gap distance. The gap modes, on the other hand, are insensitive to the nanoparticle size and are mainly determined by the facet width and gap layer thickness. Both the antenna and gap modes redshift as the gap distance is reduced (Fig. 2(e)). These modes are usually accompanied with strong field enhancement in the gap, leading to diverse promising plasmon-enabled applications.

Preparation of NPoM structures

Gold and silver are commonly chosen as plasmonic materials for their tunable properties across a wide range of wavelengths, making them a top priority in plasmonics research. Wet-chemical synthesis techniques enable the production of Au and Ag nanoparticles with diverse

shapes and sizes, which exhibit plasmon modes ranging from the ultraviolet to near-infrared region. Plasmonic Au NSs (Fig. 3(a)), with high geometrical symmetry, have been extensively used to construct NSoM structures as model demonstrations[24,25]. The resonance wavelengths of Au NSs, ranging from 520 nm to 800 nm[26], can be varied by adjusting the particle diameter. A point contact is formed between the NS and the mirror in the NSoM structure. NPoM structures composed of nanorods (Fig. 3(b)) and nanocubes (NCs) (Fig. 3(c)) have also been developed[27,28]. The nanorod-on-mirror (NRoM) and nanocube-on-mirror (NCoM) structures show a line contact and a plane contact, respectively. Compared to the NSoM, the NRoM and NCoM structures have a larger field enhancement and a smaller mode volume owing to the lower symmetries and sharper features of the nanoparticles[29]. Additionally, the {100} facets with steep inter-facet angles in the NCoM increase stability by avoiding atomic reconstruction under light illumination, while multiple atomic steps and shallow facet curvature on spherical nanoparticles can be problematic[30]. Recent research efforts have also been devoted to interesting nanoplate-on-mirror (Fig. 3(d)) and nanodisk-on-mirror (Fig. 3(e)) structures. The anapole states and plasmon-induced toroidal resonances observed in nanoplate-on-mirror structures facilitate the development of plasmonic anapole-based systems[31].

The preparation of individual NPoM structures commonly involves drop-casting, where an aqueous solution containing target nanoparticles is deposited onto

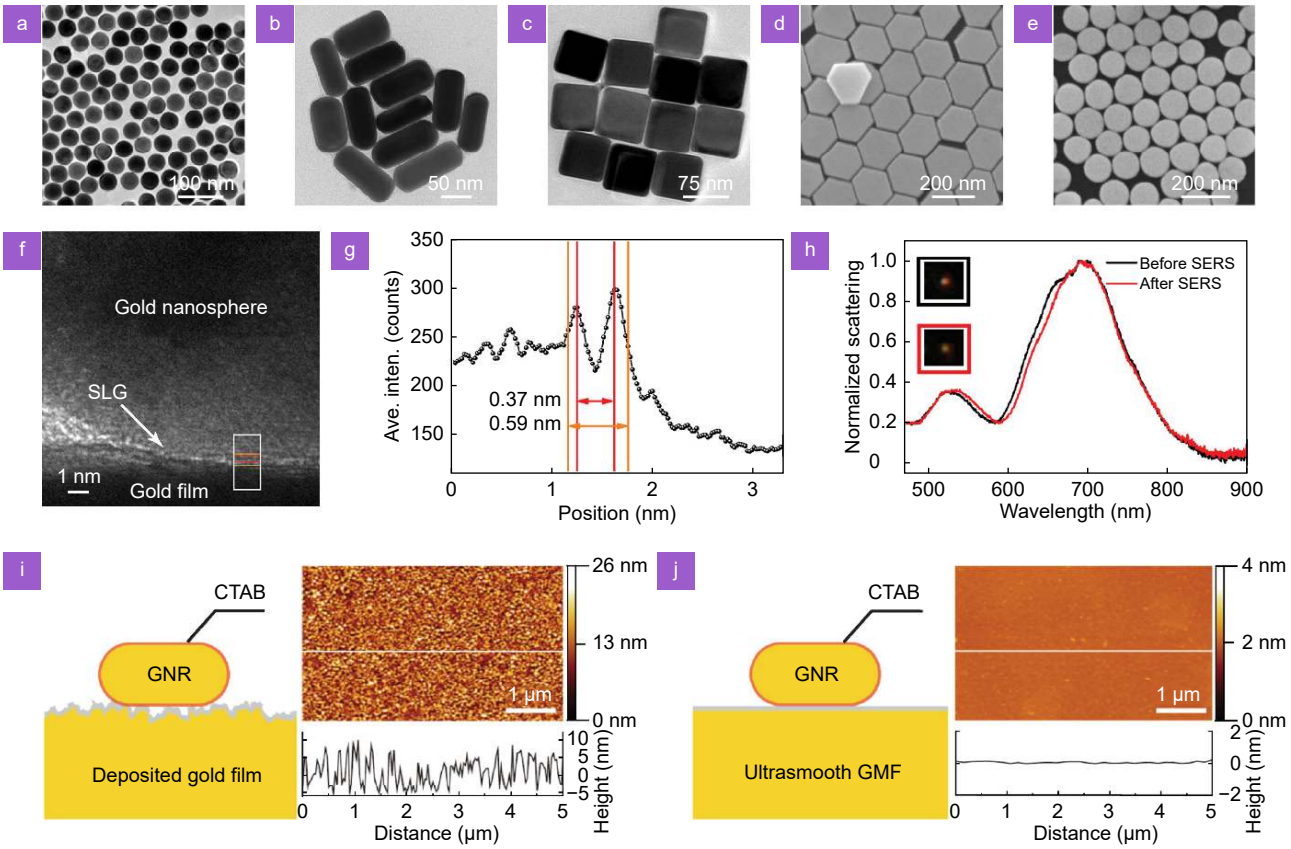

Fig. 3 | Construction of NPoM structures. (**a**–**e**) Plasmonic nanoparticles for the construction of NPoM structures: Au NSs (a), Au nanorods (**b**), Ag NCs (**c**), Au nanoplates (**d**), and Au nanodisks (**e**). (**f**) High-resolution transmission electron microscopy (TEM) cross-sectional image of a SLG-sandwiched NPoM structure. (**g**) Average count profile across the local area as indicated in the white box in (f). The values of brightness were extracted from the high-resolution TEM image in (f) for analysis. (**h**) Dark-field scattering spectra and images (insets) of the structure before and after Raman measurements. (**i**, **j**) Effect of the mirror quality: Au nanorod-on-(rough gold mirror) (i) and Au nanorod-on-(ultrasmooth gold mirror) (j). GNR: gold nanorod. The surface root-mean-square roughness of the single-crystalline gold microflake (GMF) in (j) is ~ 0.2 nm, which is much lower than that of the deposited gold film in (i). The ultrasmooth gold mirror endows the nanocavities with significantly enhanced quality factors and scattering intensities. Figure reproduced with permission from: (a) ref.[25], Copyright 2017 American Chemical Society; (b, i, j) ref.[27], Copyright 2022 American Chemical Society; (c) ref.[28], Copyright 2018 American Chemical Society; (d, e) ref.[31], Copyright 2020 Wiley-VCH GmbH; (f–h) ref.[17], Copyright 2019 American Chemical Society.

substrates with a spacer layer, followed by nitrogen-blow drying for good dispersion. Spin-coating can be an alternative method for depositing nanoparticles evenly. The removal of ligands surrounding nanoparticles is also very important. Ethanol rinsing and thermal annealing are commonly used for this purpose to improve contact. The spacer layer made of 2D materials, such as single-layer graphene (SLG), can push the gap distance to a single-atom limit (Fig. 3(f) and 3(g))[17]. Such structures are highly stable in optical measurements (Fig. 3(h)). 2D TMDCs are also widely adopted as the spacer layer and offer interesting optical properties and enhanced quantum effects, which will be discussed below.

The optical properties of a NPoM structure are highly sensitive to various factors, including the size and shape of the plasmonic nanoparticle, the properties and thickness of the gap layer, and the quality of the mirror substrate. For ideal NPoM structures, plasmonic nanoparticles with regular shapes, uniform sizes, smooth surfaces, and minimal residual ligands are preferred. Random facets of Au NSs have been reported to cause unexpected tilting of the nanoparticles when placed on mirrors, leading to nonuniform dark-field scattering spectra[25]. The surface roughness of the mirror can also affect the resonance wavelength and the consistency of the optical response across different measurements. Gold and silver films fabricated through electron-beam evaporation exhibit low roughness, while inverted Au films produced through a template-exfoliation process exhibit even lower roughness[32]. Ultrasmooth Au mirror films result in narrower linewidths for the scattering peaks from NPoM structures compared to rough Au mirror films, particularly when the Au mirror is thin[27], as shown in Fig. 3(i) and 3(j). Gold and silver microplates obtained from wet-chemical synthesis can provide ultrasmooth and single-crystalline mirror substrates, which are highly desired for low-loss plasmonics[33].

Enhanced light–matter interactions in 2D materials

Plasmon–exciton coupling from the weak to strong regime

NPoM structures with strong field enhancement and ultrasmall mode volumes offer a good platform for the study of light–matter interactions in 2D materials. Among them, plasmon–exciton coupling in TMDC-monolayer-sandwiched NPoM structures has aroused intense interest. TMDC monolayers exhibit pronounced exciton emissions with large binding energies (up to 0.9 eV[34]) and exciton transition dipole moments, which favor the interactions of the 2D excitons with the electromagnetic fields in plasmonic nanostructures. The interplay between plasmons and 2D excitons can be divided into two coupling regimes, strong and weak coupling. A coupled harmonic oscillator model (Fig. 4(a)) is usually employed to describe the strong coupling effect[35,36]. In this model, the coherent states are assumed to obey the oscillator-like motion

$$\mathrm{i}\dot{\boldsymbol{P}} = (\omega_{\mathrm{x}} - \mathrm{i}\gamma)\,\boldsymbol{P} + g\boldsymbol{E}\,, \tag{2}$$

$$\mathrm{i}\dot{\boldsymbol{E}} = (\omega_{\mathrm{c}} - \mathrm{i}\kappa)\,\boldsymbol{E} + g\boldsymbol{P}\,, \tag{3}$$

where $\boldsymbol{P}$ and $\boldsymbol{E}$ represent the excitonic contribution to the dielectric polarization and the electric field of the plasmonic resonance, respectively; $\dot{\boldsymbol{P}}$ and $\dot{\boldsymbol{E}}$ are their time derivatives; ω_{x} and ω_{c} are the angular frequencies of the exciton transition and plasmonic resonance, respectively; the subscripts 'x' and 'c' refer to the exciton and cavity; γ and κ are the dissipations of the uncoupled exciton and plasmon mode; and g is the coupling strength. The general solution of the above equations gives two eigen-frequencies ($\omega_{\pm}$) of the hybrid system

$$\omega_{\pm} = \omega_0 - \mathrm{i}(\gamma+\kappa)/2 \pm \Omega_{\mathrm{R}}/2\,, \tag{4}$$

$$\Omega_{\mathrm{R}} = \left[4g^2 - (\gamma-\kappa)^2\right]^{1/2}\,, \tag{5}$$

where Ω_{R} denotes the Rabi frequency; ω_0 represents the resonant coupling of the exciton and plasmon, that is, $\omega_{\mathrm{x}} = \omega_{\mathrm{c}} \equiv \omega_0$. Equations (4) and (5) provide the criteria for distinguishing between the two coupling regimes. In a strong coupling regime, the Rabi frequency should be real and there is $g > |\gamma - \kappa|/2$. Otherwise, the hybrid system is in a weak coupling regime. It should be noted that the damping of polariton modes $(\gamma + \kappa)/2$ can be comparable to Ω_{R} in actual cases, which makes the identification of Rabi splitting difficult. Another criterion, $\Omega_{\mathrm{R}} > (\gamma + \kappa)/2$, is also widely used to define the strong coupling regime[18,37]. Such definition is established in a pragmatic way, that is, the strong coupling occurs whenever the Rabi splitting is experimentally observable. The coupling process can be understood as the competition between the energy exchange and the system loss. When the energy exchange rate between the plasmon resonance and the exciton transition overcomes the system dissipations, strong coupling occurs, which is featured by an emerging half-light–half-matter hybridized state. The detuning of

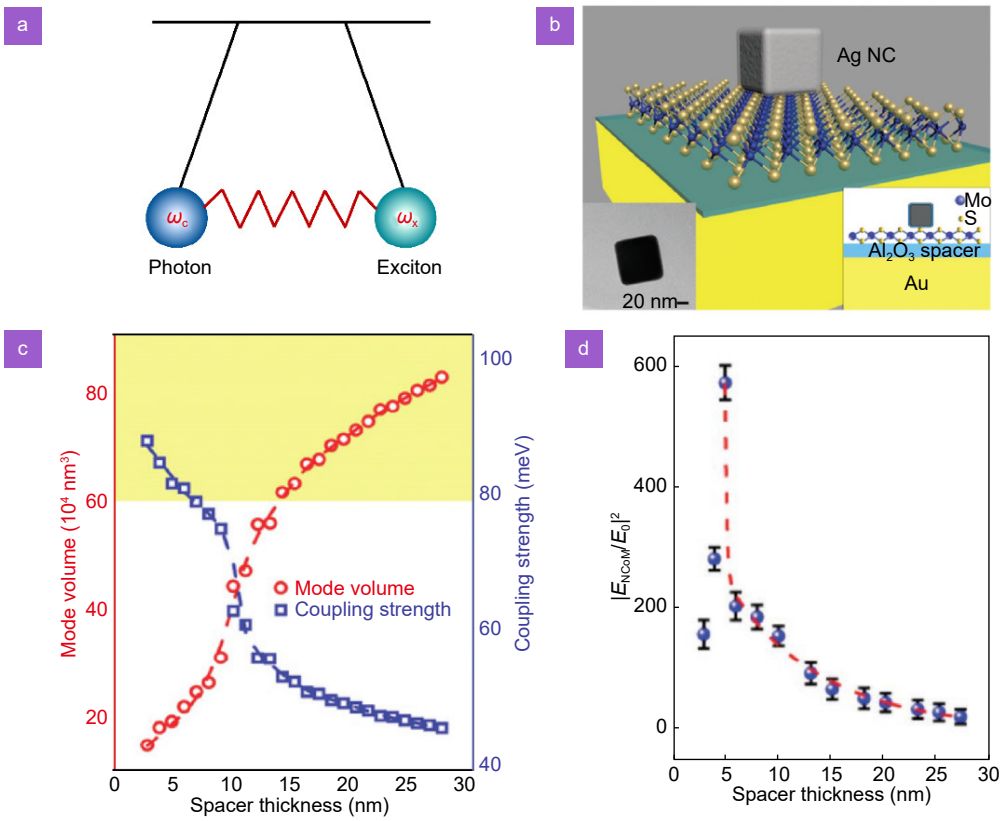

Fig. 4 | Plasmon–exciton coupling in the extreme gap. (**a**) Schematic of the coupled harmonic oscillator model. (**b**) Schematic of a NCoM structure with a MoS_2 monolayer. The insets show the TEM image of an individual Ag NC (left) and the cross-sectional schematic of the structure (right). (**c**) Dependences of the optical mode volume (red) and coupling strength (blue) on the thickness of the spacer. The strong coupling regime is shaded in yellow. (**d**) Electric field enhancement at different spacer thicknesses. Figure reproduced with permission from: (b–d) ref.[18], Copyright 2019 WILEY-VCH Verlag GmbH & Co. KGaA, Weinheim.

the plasmonic cavity and exciton transition shows a distinct anticrossing behavior in the spectral domain, with two prominent branches associated with the high- and low-energy polaritons. In contrast, the weak coupling only affects the radiative decay rate of the excitons, which is examined through the Purcell enhancement.

The strength of the coupling is determined by the exciton oscillator strength and the mode volume[37]. Specifically, the coupling strength shows an inverse square dependence on the mode volume: $g \propto 1/V^{1/2}$. In this regard, it is advantageous to exploit NPoM structures with ultrasmall mode volumes for achieving strong coupling. The thickness of the dielectric spacer can be adjusted to tailor the interaction between the nanocavity and emitters. For example, the interaction between the excitons and the plasmon resonance is pushed to the strong coupling regime by simply shrinking down the thickness of the spacer layer in a MoS_2-sandwiched NCoM structure (Fig. 4(b–d))[18]. In this structure, a Ag NC is assembled onto a piece of MoS_2 monolayer, which is separated by a Al_2O_3 layer on the Au mirror (Fig. 4(b)). When the thickness of the Al_2O_3 layer is reduced to 5 nm, two split peaks in the PL spectra are observed at room temperature, instead of a single A exciton peak from the MoS_2 monolayer on the gold film. Such energy splitting can also be found in the scattering spectra, giving rise to a larger Rabi splitting of 190 meV. The smaller splitting energy in PL is attributed to the faster polariton relaxation rate than the emission rate and the difference in splitting between absorption and scattering. When the thickness of the Al_2O_3 layer is further decreased, the mode volume becomes even smaller, which is, however, accompanied by a lower field enhancement (Fig. 4(c) and 4(d)). The suppressed field enhancement probably arises from the dramatic increase in absorption from the metal.

In contrast to NCoM, NSoM is found to be less effective for the strong coupling with the A excitons in TMDC monolayers[18,38]. For a NSoM structure sandwiched with MoS_2 or WSe_2 monolayer (Fig. 5(a)), the plasmon tuning always gives weak coupling with PL enhancement[38]. However, Rabi splitting exceeding 135 meV can be observed in multilayer structures (Fig. 5(b)

and 5(c)). The above results indicate the importance of alignment between the polarization of the dipole movement and the plasmonic mode in the gap. Other important factors include the field enhancement and mode volume. As mentioned above, nanoparticles with sharp corners induce larger field enhancement and smaller mode volumes, compared to those with spherical shapes. The advantages of nanoparticles with sharp features for strong coupling are also revealed in Au nanoprism-on-mirror structures (Fig. 5(d))[39]. A large Rabi splitting up to 163 meV in the dark-field scattering spectra and splitting features in the PL spectra are observed (Fig. 5(e)). The estimated effective exciton number contributing to the coupling reaches the single-digit level (N < 10), which is close to single-exciton-based strong coupling. We would also make comparison on strong coupling between NPoM structures and individual plasmonic nanoparticles[40–42]. Rabi splitting is only observed in the scattering spectra based on most studies using individual plasmonic nanoparticles for achieving strong coupling. In contrast, NPoM structures with ultrasmall mode volumes enable large coupling strengths to overcome the system loss. Therefore, not only scattering splitting but also PL splitting can be observed at room temperature.

In addition to strong coupling, weak coupling between plasmonic nanocavities and 2D excitons has also been widely studied. The large field enhancement in the NPoM significantly facilitates the excitation and radiative decay of 2D excitons[43–46]. This process can be approximately described using the formula <EF> = $|\boldsymbol{E}/\boldsymbol{E}_0|^2 \times (QY/QY_0)$, where <EF> is the PL enhancement factor; $|\boldsymbol{E}/\boldsymbol{E}_0|^2$ is the electric field intensity enhancement at the excitation wavelength; and QY/QY_0 is the change of the emission quantum yield, indicating the modulation of the spontaneous decay rate in the system[9]. When the quantum yield of the nanoemitter is low, the above formula can be simplified to <EF> = $|\boldsymbol{E}/\boldsymbol{E}_0|^2 \times \gamma_{PF}$, where γ_{PF} is the Purcell factor regarding the radiative decay rate of a nanoscale emitter adjacent to a nanoantenna[47]. A NCoM structure composed of a Ag NC on a Au mirror has been developed to provide both excitation and emission enhancement for the A excitons in MoS_2 monolayer (Fig. 6(a))[43]. In this structure, the MoS_2 monolayer is inserted between a 5 nm HfO_2 layer and a 1 nm polymer adhesion layer. The Ag NC is encapsulated with a 3 nm polyvinyl pyrrolidone (PVP) coating layer. The NCoM structure shows two tunable resonance modes, i.e., the dipolar mode located at 660 nm and the quadrupolar mode at 420 nm. These two modes are well separated in the spectral domain with good spatial overlap, enabling the simultaneous enhancement of the absorption and the emission quantum yield. As a result, a 2000-fold

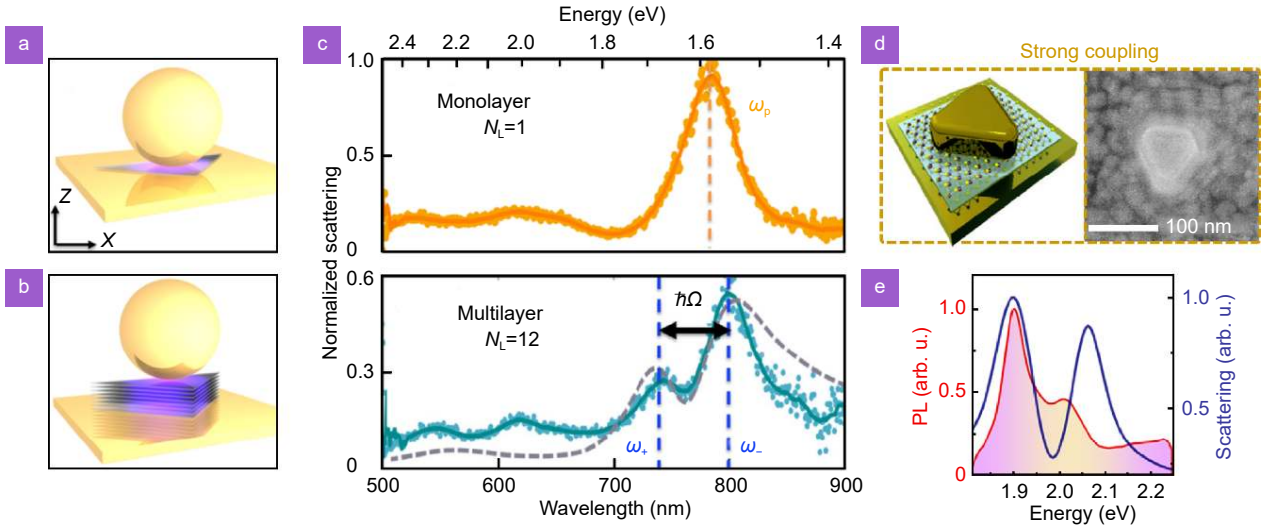

Fig. 5 | Strong coupling. (**a**, **b**) Schematics of NPoM cavities constructed from WSe_2 flakes. The layer numbers of the WSe_2 flakes are 1 (a) and 12 (b), respectively. (**c**) Dark-field scattering spectra of the individual NPoMs, showing mode splitting for WSe_2 multilayer. The mode splitting was reproduced by FDTD simulations (dashed line), with two eigen-frequencies ($\omega_\pm$) of the hybrid system and a Rabi splitting energy ($\hbar\Omega$) exceeding 140 meV. Only a single-plasmon peak was observed in the WSe_2 monolayer structure, where ω_p denotes the angular frequency of the plasmon resonance. (**d**) Schematic and scanning electron microscopy (SEM) image of a plasmonic nanocavity sandwiched with WS_2 monolayer. (**e**) PL (red) and scattering (cyan) spectra of the hybrid system in the strong coupling regime. Figure reproduced with permission from: (a–c) ref.[38], under the terms of the Creative Commons CC BY license; (d, e) ref.[39], Copyright 2020 American Physical Society.

enhancement in the PL intensity of the MoS_2 monolayer has been obtained. Ag nanowires with higher-order plasmon resonances have also been demonstrated to achieve the goal of the resonant enhancement of both absorption and PL quantum yield at the same location[46]. Moreover, polarization control of the exciton emissions can also be realized in such anisotropic systems[45].

In recent years, plasmonic nanostructures with chiral morphologies have been designed to address the valley pseudospin in 2D TMDCs at room temperature[48–52]. Chiral plasmonic nanostructures can generate chiral near-field with greater chiral asymmetry than that of circularly polarized light. TMDC monolayers inserted into the gap region experience both plasmonic field enhancement and optical chirality enhancement[48,49]. Interestingly, the conventional NCoM structure has also been found to possess local optical chirality asymmetry when the mirror symmetry is broken by slightly tilting the NC (Fig. 6(b))[50]. The left-handed (σ^-) and right-handed (σ^+) components of the PL emissions are found to be asymmetric (Fig. 6(c)), showing a relatively high room-temperature degree of valley polarization (48.7%). The valley-polarized emissions can be attributed to the chiral Purcell effect resulting from the uneven spatial distribution and lifted degeneracy of the σ^- and σ^+ photonic local density of states. The decay rate of the excitons with

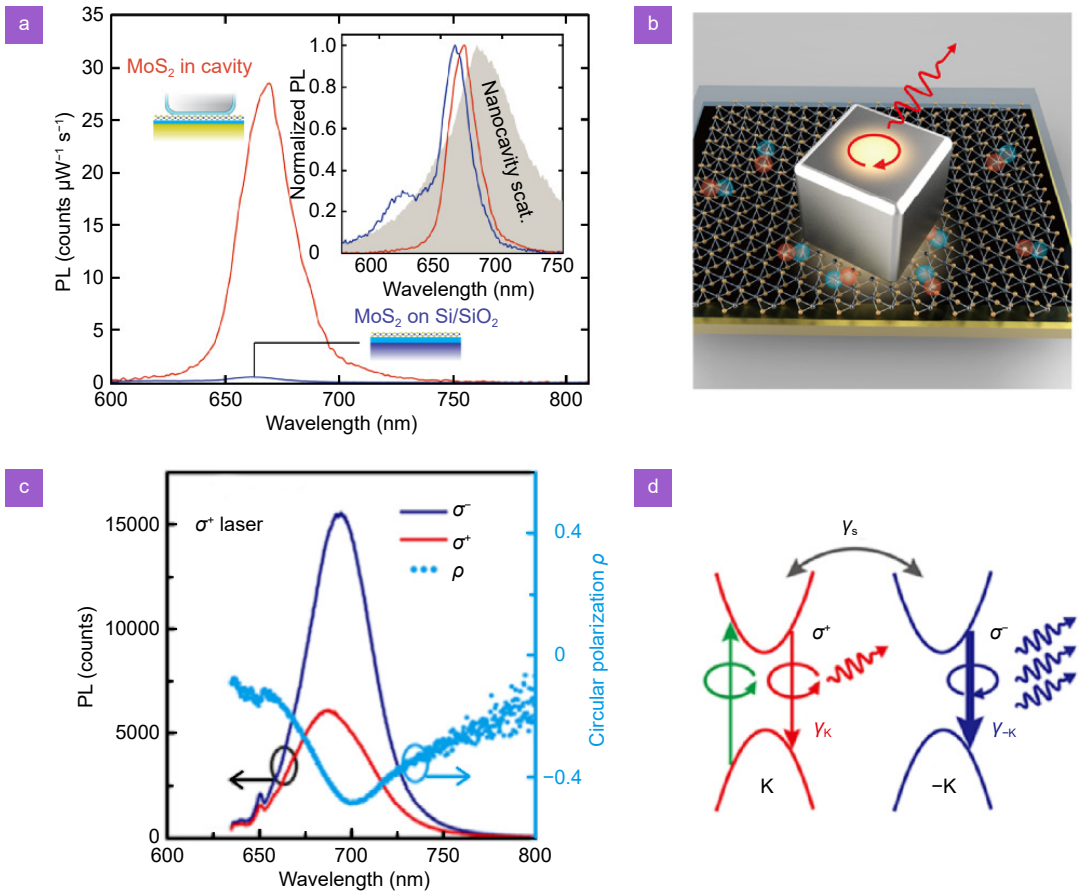

Fig. 6 | PL enhancement in the weak coupling regime. (**a**) PL spectra from a MoS_2 monolayer on a Si/SiO_2 substrate (blue) and in the nanocavity (red). The intensity is measured per unit of excitation power and per unit of integration time. The inset shows the normalized spectra for the two cases along with the scattering spectrum for a typical structure (gray). (**b**) Schematic of the MoS_2 monolayer-sandwiched NCoM structure. The Ag NC is wrapped with PVP and separated from an ultrasmooth gold film by an alumina layer and a MoS_2 monolayer. (**c**) Circularly polarized PL spectra under the right circularly polarized (σ^+) excitation. The degree of circular polarization, defined as $\rho = (I(\sigma^+) - I(\sigma^-))/(I(\sigma^+) + I(\sigma^-))$, was used to evaluate the valley modulation. $I(\sigma^+)$ and $I(\sigma^-)$ are the measured right-handed and left-handed components of the PL emissions, respectively. A high degree of circular polarization up to 48.7% was obtained. (**d**) Schematic showing the valley-dependent emissions owing to the chiral Purcell effect. The decay rate of the excitons in the –K (γ_{-K}) valley is much larger than that in the K (γ_K) valley, leading to enhanced left-handed PL emissions. The intervalley scattering process is denoted using the parameter (γ_s) with a similar expression to the decay rate of the excitons. Figure reproduced with permission from: (a) ref.[43], Copyright 2015 American Chemical Society; (b–d) ref.[50], Copyright 2020 American Chemical Society.

different valley indexes can therefore be separately modulated, leading to remarkably enhanced valley polarization (Fig. 6(d)).

Plasmonic nanocavities with large field enhancement also offer a feasible tool for probing diverse excitonic complexes in addition to neutral A excitons, such as B excitons[53], dark excitons[54,55], localized excitons[13,56], and interlayer excitons[57]. These types of 2D excitons are usually inaccessible under normal conditions owing to their low quantum yields. For instance, the NCoM structure is employed to create dominant B exciton emissions in MoS_2 monolayer (Fig. 7(a))[53]. The B excitons in MoS_2 monolayer are associated with the optical transitions from the lower valence band to the bottom of the conduction band. A 6100-fold enhancement of the B exciton emissions is observed when spectral resonant matching is realized. More importantly, the gap plasmon modes of NPoM structures provide significant out-of-plane field enhancement, which is believed to be critical for the detection of 2D excitons with out-of-plane dipole moments. The probing of spin-forbidden dark excitons is a typical example of this aspect. The spin-forbidden dark excitons correspond to the optical transition from the higher-lying valence band to the split conduction band with an anti-parallel spin configuration. This type of dark exciton shows orthogonal transition dipole orientation with the A excitons and is generally hard to excite and detect in conventional optical measurements. The radiative decay rate of the dark excitons in WSe_2 monolayer has recently been shown to be enhanced by nearly 6 orders of magnitude through the Purcell effect in a NSoM structure (Fig. 7(b))[55]. The PL intensity of the dark excitons clearly outperforms that of the spin-allowed bright excitons (Fig. 7(c)), when the background emissions are removed through the etching of the uncoupled WSe_2 region. The above results indicate that the plasmonic field in the NPoM structure can extract electronic transitions before the spin flip under thermal excitation. This simple device structure offers a facile approach for manipulating the dark states by avoiding the use of extreme experimental conditions, such as cryogenic temperatures[58], ultrahigh in-plane magnetic field[59], and tip-enhanced techniques[54]. Interlayer excitons from layered TMDC heterostructures are another type of 2D exciton with out-of-plane dipole moments. The integration of the interlayer excitons in WS_2/MoS_2 stacking into plasmonic nanocavities based on Ag NCs gives rise to an order of magnitude PL enhancement at room temperature and a 5-time enhancement at cryogenic temperatures (Fig. 7(d) and 7(e))[57]. The plasmonic techniques also promise to manifest the fine structures of moiré excitons, which requires further investigation.

2D TMDCs are also an excellent platform for the observation of phonon-assisted upconversion owing to the enhanced optical transition strength and interaction of the 2D excitons with phonons. The anti-Stokes process is activated through the creation of resonant conditions, that is, the incident or/and emitted photon energy matches the resonance level of the material system. A series of excitonic states, including spin-triplet trions, spin-singlet trions, and intravalley (spin-forbidden) dark excitons, can be upconverted to the bright excitons under resonant conditions[60–62]. Plasmonic nanocavities are integrated to change the local optical environment. For example, the broad plasmon resonance from a Au NCoM structure is coupled to the excitation laser light at 1.52 eV and the emissions at 1.65 eV in WSe_2 monolayer (Fig. 8(a–c))[61]. An upconverted emission amplification exceeding 1000 times and a reduction of 2–3 orders of magnitude in the saturated excitation power are achieved. The temperature-dependent spectra (Fig. 8(d)) show evidence for the involvement of phonons in the upconversion process. In one most recent work, phonon-assisted upconversion in WSe_2 monolayer is obtained through the resonant excitation of the intravalley dark excitons at room temperature[62]. It is also proposed that the precise control of the nanoparticle geometry is important for reducing the variation in the anti-Stokes PL enhancement. The decahedral nanoparticle shape is found to provide a 10-fold narrower distribution of the enhancement factor for the anti-Stokes PL, compared to NSoM structures. The upconverted PL can be further modulated reversibly by electrochemical gating.

Surface-enhanced Raman scattering (SERS) in the nanocavity

Raman scattering arises from the inelastic scattering of light by phonons, which are quantized states of vibrations in solids and molecules. Raman spectroscopy has become a fast and nondestructive method to characterize the physical and optical properties of 2D materials[63,64]. Rich information about the lattice vibrations of 2D materials can be revealed through the analysis of the line shape, linewidth, peak position, and intensity, which helps to uncover microscopic processes such as electron–phonon coupling[65], strain dependence for

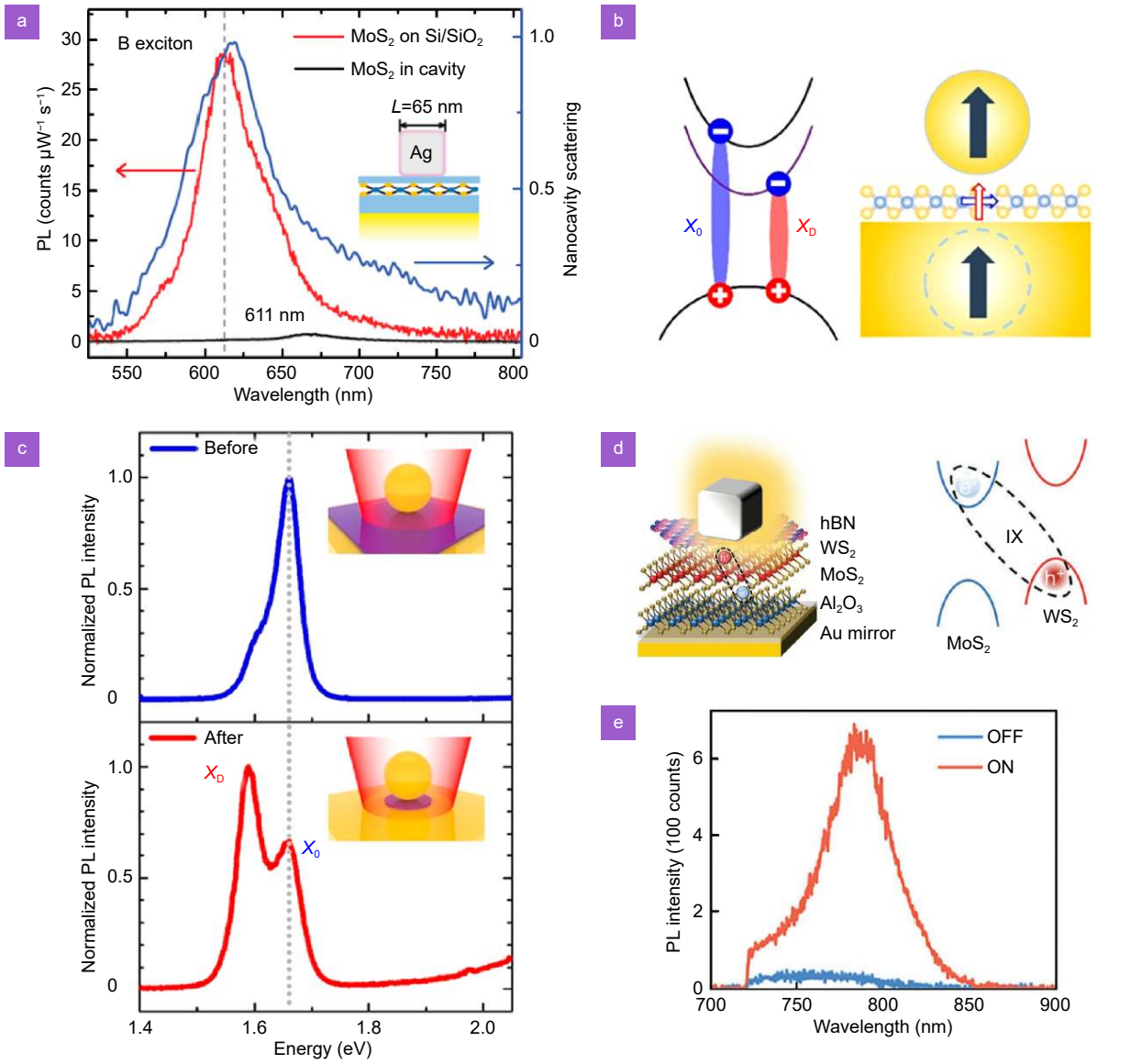

Fig. 7 | Plasmonic enhancement for the detection of new exciton complexes. (**a**) PL spectra from a MoS_2 monolayer on Si/SiO_2 (black) and a MoS_2 monolayer in the nanocavity containing a 65 nm Ag NC (red). The B exciton emissions are largely enhanced. (**b**) Schematic showing the bright (X_0) and dark excitons (X_D) in the WSe_2 monolayer at the K valley (left) and the coupling between the gap plasmon mode of NSoM and the out-of-plane dipole of the dark excitons (right). (**c**) PL spectra obtained from the unetched WSe_2-NSoM (top) and etched WSe_2-NSoM (bottom). The insets show the corresponding nanostructures. The PL peak related to the dark excitons is clearly seen in the etched structure. (**d**) Schematic of a WS_2/MoS_2 heterostructure inserted in a NPoM cavity. A thin h-BN flake acts as a spacer to adjust the resonance wavelength to match the interlayer emissions. The type II band alignment is shown in the right panel, forming the interlayer excitons (IX). (**e**) PL spectra from the coupled (red) and uncoupled structures (blue). Figure reproduced with permission from: (a) ref.[53], Copyright 2017 American Chemical Society; (b, c) ref.[55], Copyright 2022 American Chemical Society; (d, e) ref.[57], Copyright 2021 Wiley-VCH GmbH.

elastic constants[66], and quantum interference in Raman scattering processes[67]. Plasmonic nanostructures are highly active in enhancing Raman scattering on 2D materials based on two reasons. First, the efficiency of Raman scattering is very low, that is, typically one in every ~10^5–10^7 photons produces a Raman-scattered photon[63]. Second, the light–matter interaction length in 2D materials is at the subnanometer scale, leading to low absorption of light compared to the bulk materials. Here we focus on SERS in (2D material)-sandwiched NPoM structures. The measured SERS enhancement factor is well known to follow the fourth power of the local electric field enhancement, which is also called the E^4 law[68]. The plasmonic cavity is thus a magnifier to monitor any subtle change in the phonon response of the 2D system. In turn, the vibrational modes of 2D materials can also be a

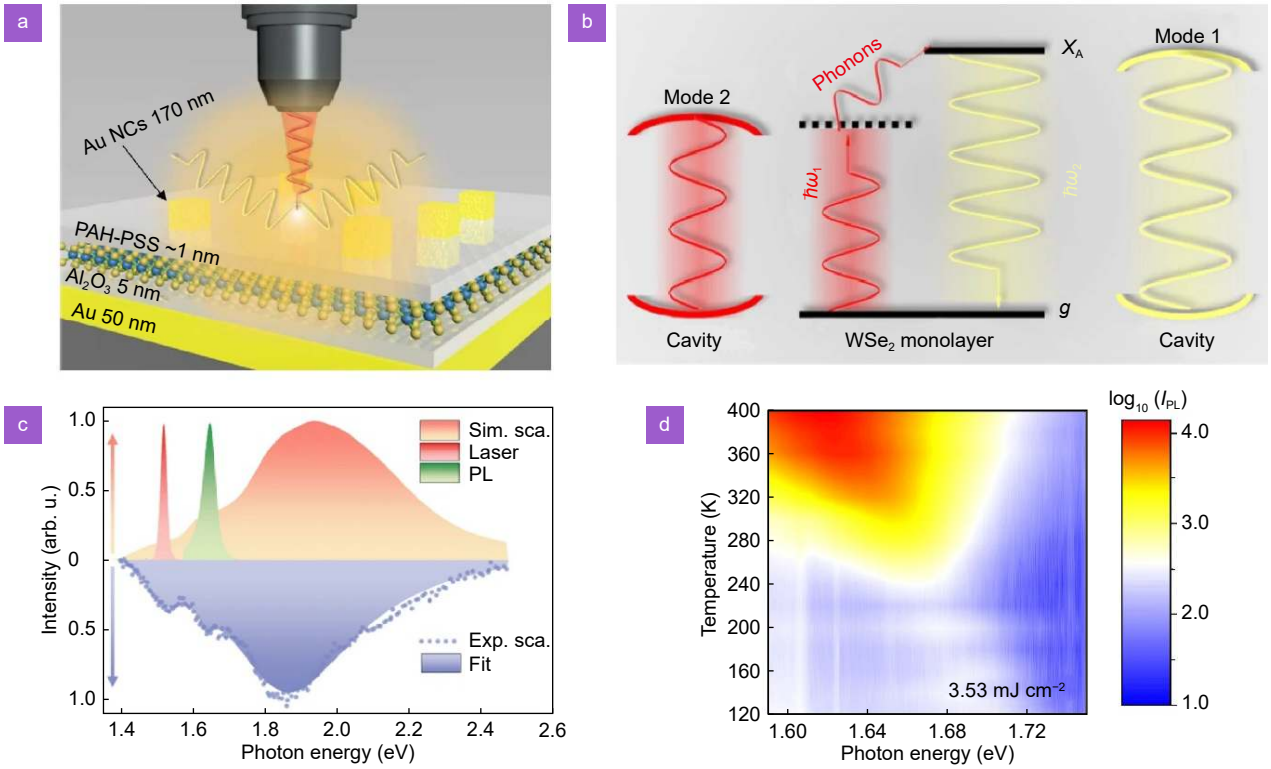

Fig. 8 | Excitonic upconverted emissions. (**a**) Schematic of the plasmonic nanocavity. The WSe_2 monolayer is separated from the Au NCs with an organic adhesive layer, i.e., poly(allylamine hydrochloride)/poly(sodium 4-styrenesulfonate) (PAH-PSS), to avoid the hot carrier injection from the plasmonic nanoparticles. (**b**) Energy diagram showing the photon upconversion process of the 2D excitons. The electrons in the ground state (g) are excited through the absorption of a photon with energy ($\hbar\omega_1$) and pumped to a higher energy state (X_A) through the absorption of phonons (red arrow). The formed excitons are then recombined through the emissions of upconverted photons with energy ($\hbar\omega_2$). The plasmonic nanocavities provide two cavity modes for double resonance with the incident and emitted photon energies to achieve both excitation and emission enhancement. (**c**) Spectra corresponding to the excitation laser light, PL emissions of WSe_2 monolayer, and dark-field scattering of the hybrid structure. (**d**) Temperature-dependent upconverted emissions, indicating the influence of phonons. Figure reproduced with permission from: ref.[61], under a Creative Commons Attribution 4.0 International License.

probe to sense the local field enhancement in the nanocavity. For example, the quantitative SERS intensities of graphene and TMDC monolayer have been used to test the ultimate limit of plasmonic enhancement within a subnanometer gap[17,24,69]. For a MoS_2-NPoM structure, the intrinsic out-of-plane (A_{1g}) and in-plane (E^1_{2g}) lattice vibrations of the MoS_2 monolayer are softened, with two new peaks (labelled as $A_{1g}{}'$ and $E^1_{2g}{}'$) showing up owing to the doping and strain effects from the metallic contact (Fig. 9(a–c))[24]. Both the out-of-plane components (A_{1g} + $A_{1g}{}'$) and in-plane components (E^1_{2g} + $E^1_{2g}{}'$) are largely enhanced in the MoS_2-NPoM structure. The out-of-plane and in-plane vibrational modes are aligned with the perpendicular and horizontal local fields, respectively. The SERS enhancement of these two modes (EF_{xy} and EF_z) can therefore be used to quantitatively probe the local field enhancement in the two orthogonal orientations. Based on the spectroscopic analysis, the out-of-plane field enhancement (EF_z) in the gap region is much larger than the in-plane field enhancement (EF_{xy}). The value of EF_z is found to rapidly increase as the gap becomes narrower, reaching up to 5.1×10^8 for a MoS_2 monolayer structure. The in-plane near-field enhancement when the gap distance is below 1 nm is, however, lower than expected. Electron tunneling is predicted in such a subnanometer gap. A recent work shows that the h-BN monolayer is a good dielectric spacer to block electron tunneling, extending the ultimate plasmonic enhancement limit in the classical framework in a single-atom-layer gap[70]. TMDC monolayer has also been embedded at different positions in the gap region to show the field distribution in the nanocavity[71,72]. For example, WS_2 monolayer is stacked in different orders with four layers of MoS_2 using the PMMA layer-by-layer transfer method and placed inside a NSoM structure[71]. The quantitative SERS intensity of the WS_2 monolayer

located at different layer positions is used to measure the plasmonic field distribution. The plasmonic field in the nanocavity is found to be heterogeneous, with a maximal value close to the nanoparticle and a minimal value in the middle of the gap. The above investigations have demonstrated 2D materials as a good probe. They can be easily integrated into the "hotspot" and support vibrational modes with certain orientations.

Nonlinear effects can also be observed in the SERS measurements of the MoS_2-NPoM structure[19]. An anomalous superlinear power dependence of the SERS intensity of the A_{1g} mode appears when the excitation wavelength is blue-detuned to the plasmonic resonance (Fig. 9(d–f)). This superlinear behavior is attributed to the dynamic backaction modification of the phonon population, that is, the pumping rate of phonons modulated by the plasmonic field is larger than the damping rate. Another phenomenon related to the nonlinear effect is the significantly large Raman scattering of the second-order Raman-inactive phonon mode 2LA (LA: longitudinal acoustic), which is round-trip scattering by two LA phonons (Fig. 9(b)). The 2LA mode is extremely weak compared with the first-order Raman-active phonon modes A_{1g} and E^1_{2g} if the plasmonic enhancement is absent. The 2LA mode also shows superlinear power-dependent behavior and surpasses the A_{1g} mode at large excitation intensities.

Quantum tunneling in the extreme gap

As the plasmonic nanocavity comes to the subnanometer range, the plasmon resonance enters the quantum regime. The quantum mechanical effects of plasmon resonance arise from the nonlocal screening of electrons and electron tunneling through the gap when the gap distance continues to shrink[73]. Classical electromagnetic treatments fail at this regime and the plasmonic properties of the cavity can be completely modified by electron tunneling. Quantum tunneling induces blueshifts in the plasmon resonance, reduces the local field enhancement, and generates charge-transfer plasmons[73,74]. The tunneling plasmonics not only pushes fundamental research to a new frontier but also brings potential applications in the ultimate miniaturization of photonic components for quantum optics[75], nanoreactors[76], and biosensing with single-molecule sensitivity[77]. However, it has been challenging to fabricate quantum plasmonic nanocavities

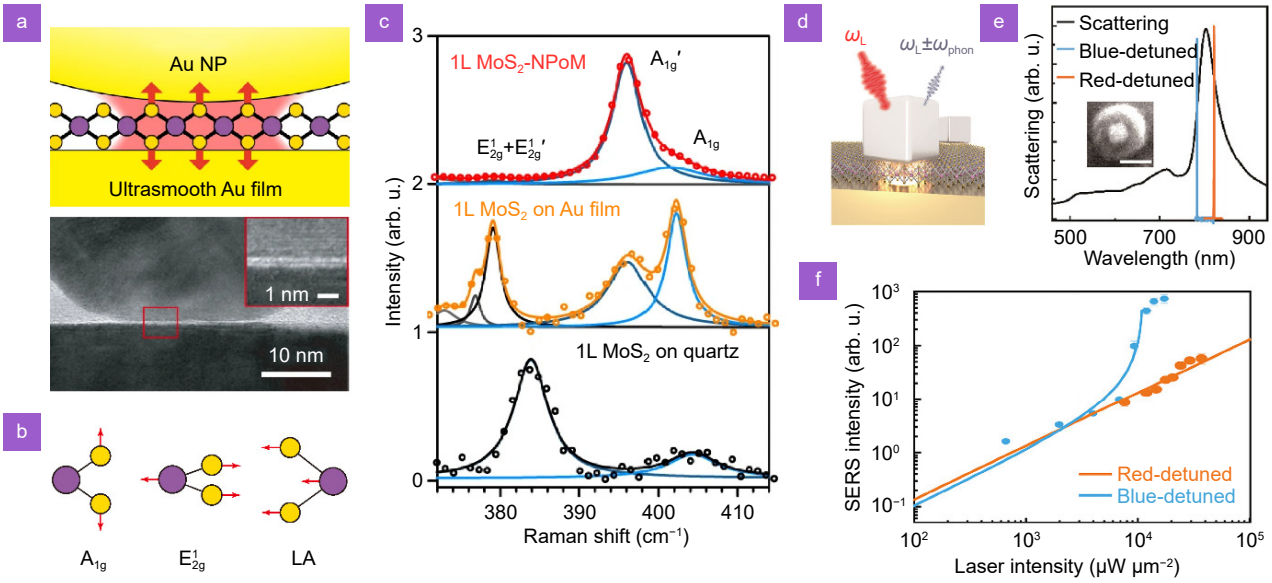

Fig. 9 | Surface-enhanced Raman scattering. (**a**) Schematic (top) and cross-sectional TEM image (bottom) of a 1L MoS_2-NPoM structure. The inset in the bottom panel shows the enlarged image of the marked area (red square). (**b**) Atomic displacements of the A_{1g}, E^1_{2g}, and LA modes in the unit cell of MoS_2 monolayer. (**c**) Normalized Raman spectra of 1L MoS_2-NPoM, 1L MoS_2 on a Au film, and 1L MoS_2 on a quartz substrate. In the 1L MoS_2-NPoM cavity, the MoS_2 monolayer is coated with a 32-nm-thick Al_2O_3 layer. (**d**) Schematic showing the pumping process of a MoS_2-spaced NCoM system under laser light excitation (ω_L). The plasmonic nanocavity is designed to selectively enhance the Stokes ($\omega_L - \omega_{phon}$) or anti-Stokes ($\omega_L + \omega_{phon}$) processes. (**e**) Scattering and laser light spectra (blue line, 784 nm; orange line, 821 nm) in the blue-detuned and red-detuned measurements, respectively. The inset shows the SEM image of the tested sample (scale bar: 100 nm). (**f**) Power-dependent SERS intensity for the A_{1g} mode, showing a drastic increase in the blue-detuned case. Figure reproduced with permission from: (a–c) ref.[24], under a Creative Commons Attribution 4.0 International License; (d–f) ref.[19], Copyright 2022 American Chemical Society.

with subnanometer gaps in a reliable and repeatable manner with state-of-the-art technologies. 2D materials with atomic thicknesses can provide solutions to the challenges of fabricating quantum plasmonic devices and controlling plasmons by electronic means. Electron tunneling mediated by MoS_2 monolayer has been predicted in a work where the in-plane near-field enhancement limit is probed by SERS[24]. Simulations based on classical electromagnetics have been found to be able to precisely estimate the plasmonic enhancement until the gap distance is narrowed to ~ 1 nm (Fig. 10(a)). The measured field enhancement is ~ 38.4% lower than the calculated one when the gap distance is below 1 nm. After the reliability of the experimental design is taken into account, the quenching of the field enhancement is believed to arise from electron tunneling across the MoS_2 monolayer. In addition to MoS_2 monolayer, graphene has also been reported to change the plasmonic response of the nanocavity[20,78]. Spectral doublets from the coupled dimer modes are observed with single-layer graphene as a spacer and disappear for increasing numbers of layers (Fig. 10(b) and 10(c)). The spectral features are believed to correlate with the charger-transfer-sensitive gap plasmons. However, there have been only a few experimental demonstrations of using 2D materials as the conductive gap, especially compared with their molecular counterparts. The problems probably lie in the large out-of-plane resistance of 2D materials and the unavoidable van der Waals gap, which can form a tunnel barrier to block electrons[79]. For example, an air gap is observed between the graphene layer and the mirror possibly owing to the gold film roughness, relaxed van der Waals forces, or the wrinkling of the graphene monolayer[17]. The exploration of a process or a structure to form a good electrical contact between 2D materials and metallic nanostructures is therefore very important.

Applications of (2D material)-sandwiched NPoM structures

Hybrid nanostructures composed of 2D materials and plasmonic nanocavities have been demonstrated to be an excellent platform for the fundamental investigation of light–matter interactions, as discussed above. Their intriguing characteristics can be used for promising applications, especially in nanoscale luminescent sources. Single-photon sources based on 2D TMDCs have attracted great interest for future quantum optical applications[13,80–82]. Plasmonic nanocavities have been employed to enhance single-photon emissions in TMDC monolayers. The effect of a plasmonic nanocavity on

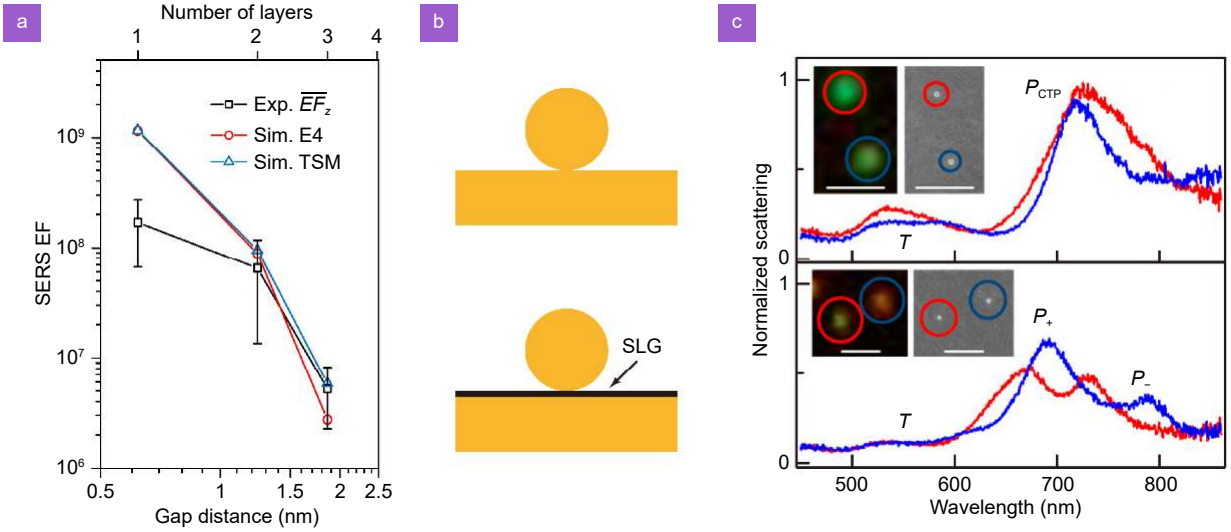

Fig. 10 | Quantum tunneling through the atomic spacer. (**a**) Measured (Exp. $\overline{EF_z}$) and simulated maximal field enhancement in response to the gap distance in a 1L MoS_2-NPOM structure. The simulated field enhancement factors were calculated using the E^4 model (Sim. E^4) and the two-study model (Sim. TSM), respectively. The reduction of the measured plasmonic enhancement in the atomic gap suggests the emergence of the quantum tunneling effect. (**b**) Schematics showing two types of structures, Au NS on a Au film without (top) and with (bottom) SLG as a spacer. (**c**) Single-particle dark-field scattering spectra of the two types of structures in (b). The corresponding dark-field images (left) and SEM images (right) are given in the insets. The transverse (*T*) and charge transfer (P_{CTP}) plasmon modes are seen when the Au NSs are in direct contact with the Au film. Interestingly, the plasmon doublet (P_+ and P_-) appears in the SLG-sandwiched structure, which is believed to arise from the hybridization of the charge transfer plasmon mode and the gap mode. The scale bar is 1 μm. Figure reproduced with permission from: (a) ref.[24], under a Creative Commons Attribution 4.0 International License; (b, c) ref.[20], Copyright 2013 American Chemical Society.

TMDC single-photon emitters can be twofold: strain localization and electromagnetic enhancement. For example, a lithographically defined Au NC array is fabricated and pressed onto a WSe_2 monolayer, with the sharp corners of the Au NCs to both provide large electric field enhancement and apply local strain on 2D TMDCs (Fig. 11(a) and 11(b))[13]. The Purcell factors of up to 551, with an average of 181, are obtained for a 3 × 4 array of quantum emitters. As a result, the brightness of the single-photon emissions is largely enhanced, without affecting the single-photon purity. A representative zero delay time value of $g^{(2)}(0) = 0.15 \pm 0.03$ (Fig. 11(c)) and an average $g^{(2)}(0)$ well below 0.5 from 15 tested structures (Fig. 11(d)) confirm pronounced single-photon antibunching. The single-photon emission rates of up to 42 MHz and a narrow exciton linewidth as low as 55 μeV are further demonstrated at the cryogenic temperature of 3.8 K. A few recent works have further shown the possibility for room-temperature observation of strain-localized emissions through the optimization of plasmonic enhancement[83,84]. However, the single-photon emissions from 2D TMDCs at room temperature have not yet been demonstrated. Negatively charged boron vacancy (V_B^-) defects in h-BN with optically addressable spin states are also good candidates for quantum optical applications such as ultrathin quantum sensors[85,86]. Integrating V_B^- defects in h-BN with plasmonic NPoM structures raises the overall intensity enhancement up to 250 times, along with preserved optically detected magnetic resonance contrast[86]. NPoM structures have also found promising applications in electroluminescent devices. A van der Waals quantum tunneling device has been combined with a Ag NC-on-Au mirror structure[87]. The photon generation is created from the inelastic electron tunneling through the van der Waals heterostructure. It exhibits a broad emission peak. The plasmonic nanocavity enables a resonant enhancement of the photon emission rate in a narrow frequency band by four orders of magnitude. The NPoM nanocavities in these devices serve as a medium to amplify the weak signals from the nano-emitters through the weak coupling effect, which benefits in avoiding strict application requirements. The strong coupling between plasmonic nanocavities and 2D materials is also expected in applications such as tresholdless lasing[88], which requires further study.

The (2D material)-sandwiched NPoM structures can

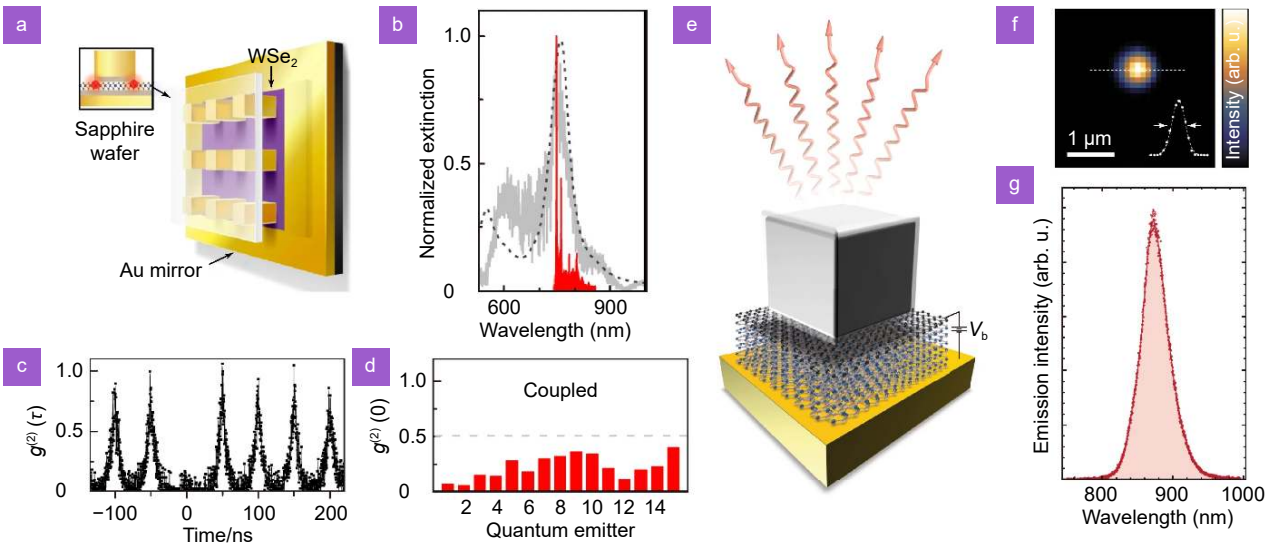

Fig. 11 | 2D material-gapped nanocavities for nanoscale light sources. (**a**) Schematic of WSe_2 monolayer coupled to a Au NCoM array for single-photon emissions. The inset shows the cross-sectional view of the structure. The WSe_2 monolayer is separated from the Au NCs and the Au film by a 2 nm Al_2O_3 layer (grey shading in the inset) on each side to prevent quenching and short-circuiting of the nanoplasmonic gap mode. (**b**) Simulated (dashed line), measured (grey solid line) extinction spectra, and emission spectrum (red solid line) of an individual quantum emitter. (**c**) Second-order photon-correlation function $g^{(2)}(\tau)$ recorded under pulsed excitation, indicating single-photon emissions. (**d**) Single-photon purity values at zero delay time for 15 quantum emitters. (**e**) Schematic showing an electroluminescence device. A PVP-coated Ag NC is separated from a Au film by a graphene (top) and h-BN (bottom) stacking. (**f**, **g**) Measured spatial (f) and spectral (g) photon distributions. The inset in (f) shows a line-cut of the emission spot, featuring a linewidth of ~ 460 nm. Figure reproduced with permission from: (a–d) ref.[13], Copyright 2018 The Author(s), under exclusive licence to Springer Nature Limited; (e–g) ref.[87], Copyright 2019 The Author(s), under a Creative Commons Attribution 4.0 International License.

also find potential applications in sensing. We have mainly discussed the intensified SERS signals of 2D materials above. The SERS signals are amplified by the electromagnetic enhancement from the plasmonic nanocavities in these structures. The 2D materials themselves can also serve as SERS substrates to provide chemical enhancement for molecular sensing[89]. The principle is based on the charge transfer effect, which is the formation of charge-transfer complexes between adsorbed molecules and substrates. The utilization of (2D material)-sandwiched NPoM structures is believed to be able to combine charge transfer enhancement and electromagnetic enhancement for molecular sensing. In addition, NPoM structures have been employed to achieve chiral sensing of single molecules in a recent work[77]. Interestingly, tunneling electrons are found to provide an additional enhancement to the chiral sensitivity. The (2D material)-sandwiched NPoM structures can also function as a good platform for chiral sensing. In the (2D material)-sandwiched NPoM structures, active control can possibly be realized by switching on and off the tunneling channel through the doping of the intermediate 2D material[90]. Hot electrons that are generated from the plasmonic nanoparticle and penetrate through the 2D material can also be used to trigger photocatalytic reactions[10]. The utilization of a graphene monolayer as the gap material has been found to increase the hot-electron transfer efficiency by over three times.

Summary and outlook

NPoM structures can support much stronger optical confinement compared to individual plasmonic nanoparticles, making them a good platform for the investigation of light–matter interactions in 2D materials. In this review, we have overviewed the important research progress in the integration of NPoM structures with 2D materials. First, we have briefly introduced the cavity modes and the important factors that affect the optical properties of NPoM structures. Second, we have examined in detail plasmon-modulated light–matter interactions in 2D materials. The important structural parameters to modulate 2D excitons from the strong coupling to weak coupling regimes have been elucidated. The SERS measurements as well as the quantitative study of the near-field enhancement in the nanogap have been presented. Third, we have discussed the possible quantum effects of the extreme gap. Fourth, we have shown the potential applications, especially for nanoscale light sources. We can see that the plasmonic strategy helps to reveal the rich microscopic processes in the 2D system. 2D materials, in turn, provide new functionalities for plasmonic control. For example, graphene has been employed as a mirror substrate to achieve plasmon confinement down to the ultimate limit of the length scale of one atom in the mid-infrared region[91]. The use of graphene is attractive for suppressing optical loss, which is large in metals due to Landau damping.

We finally would like to point out unanswered questions and future directions for the combination of NPoM structures and 2D materials in four aspects. (1) Strong coupling. Mode splitting in the PL spectra has been observed in TMDC monolayers embedded into NPoM structures, indicating the emergence of ultrastrong coupling. The ultrastrong coupling can be a good probe to reveal coherent processes in 2D TMDCs. For example, the formed exciton–polaritons in a microcavity have been demonstrated to maintain the valley properties of their excitonic component[92–94]. Moreover, valley-coherent exciton–polaritons can be addressed[95,96], with the degree of the valley coherence of the quasiparticles exceeding 90% upon excitation through a two-photon absorption process[96]. A coherent phonon scattering process in MoS_2 monolayer has also been demonstrated under the strong coupling regime[97]. The strong coupling between the phonon modes and the plasmonic cavity modes enables a drastically enhanced valley polarization (2.5 times) in the Raman scattering spectra. These findings provide a good reference for future exploration of more fundamental polaritonic processes in the 2D system, which will certainly boost an in-depth understanding of the valley-polarized properties of the exciton–polaritons modulated by the strong plasmonic field. In addition, more effort should be made to clarify the critical structural parameters for achieving ultrastrong coupling. (2) Weak coupling. The large plasmonic field enhancement in NPoM structures has been successfully employed to detect various excitonic complexes. More efforts are encouraged to achieve a new dimension of control. For example, a tilted NCoM structure with chiroptical response has been coupled to rare-earth-doped nanoparticles to achieve up-converted PL chirality[98]. Compared to tilted NCoM structures, (chiral NC)-on-mirror structures provide a more controllable way to modulate and amplify chiroptical signals[99]. Future studies are encouraged to integrate versatile 2D materials with the new type of chiral nanocavities for plasmonic modulation of

valley excitons and moiré excitons. The cavity-dependent circularly polarized single-photon emissions in 2D TMDCs[100] is also very interesting and more research efforts are desired. (3) Quantum tunneling. There has still been a lack of experimental evidence for confirming the electron tunneling in the ultimate gap formed by single-layer 2D materials. As discussed above, the large out-of-plane resistance and the air gap are the possible reasons for hindering electron tunneling. Further investigations on the quantum tunneling enabled by 2D materials and its active control are highly desired. (4) Exploration for more possibilities. Most of the current research efforts focus on the study of individual NPoM structures. Plasmonic superlattices composed of arrays of nanoparticles can provide lattice resonance modes for plasmonic modulation. For example, Au superlattices have been found to support multiple band-edge modes. The integration of Au superlattices with appropriate gain materials has enabled population inversion at plasmonic hotspots and multi-modal nanolasing[101]. Moreover, the development of robust and reproducible fabrication techniques for plasmonic nanostructures will be crucial for practical applications.

In all, we believe advances in this field will provide more insight into the plasmonic control of 2D materials and facilitate new nanophotonic applications.

References

1. Xia FN, Wang H, Xiao D et al. Two-dimensional material nanophotonics. *Nat Photonics* **8**, 899–907 (2014).
2. Grigorenko AN, Polini M, Novoselov KS. Graphene plasmonics. *Nat Photonics* **6**, 749–758 (2012).
3. Schaibley JR, Yu HY, Clark G et al. Valleytronics in 2D materials. *Nat Rev Mater* **1**, 16055 (2016).
4. Pei JJ, Liu X, del Águila AG et al. Switching of K-Q intervalley trions fine structure and their dynamics in n-doped monolayer WS_2. *Opto-Electron Adv* **6**, 220034 (2023).
5. Xia FN, Wang H, Jia YC. Rediscovering black phosphorus as an anisotropic layered material for optoelectronics and electronics. *Nat Commun* **5**, 4458 (2014).
6. Dai S, Fei Z, Ma Q et al. Tunable phonon polaritons in atomically thin van der Waals crystals of boron nitride. *Science* **343**, 1125–1129 (2014).
7. Kang K, Lee KH, Han YM et al. Layer-by-layer assembly of two-dimensional materials into wafer-scale heterostructures. *Nature* **550**, 229–233 (2017).
8. Sierra JF, Fabian J, Kawakami RK et al. Van der Waals heterostructures for spintronics and opto-spintronics. *Nat Nanotechnol* **16**, 856–868 (2021).
9. Ming T, Chen HJ, Jiang RB et al. Plasmon-controlled fluorescence: beyond the intensity enhancement. *J Phys Chem Lett* **3**, 191–202 (2012).
10. Yang JL, Wang HJ, Zhu ZW et al. In situ Raman probing of hot-electron transfer at gold–graphene interfaces with atomic layer accuracy. *Angew Chem Int Ed* **61**, e202112749 (2022).
11. Lu RT, Konzelmann A, Xu F et al. High sensitivity surface enhanced Raman spectroscopy of R6G on *in situ* fabricated Au nanoparticle/graphene plasmonic substrates. *Carbon* **86**, 78–85 (2015).
12. Gong SH, Alpeggiani F, Sciacca B et al. Nanoscale chiral valley-photon interface through optical spin-orbit coupling. *Science* **359**, 443–447 (2018).
13. Luo Y, Shepard GD, Ardelean JV et al. Deterministic coupling of site-controlled quantum emitters in monolayer WSe_2 to plasmonic nanocavities. *Nat Nanotechnol* **13**, 1137–1142 (2018).
14. Schuknecht F, Kołątaj K, Steinberger M et al. Accessible hotspots for single-protein SERS in DNA-origami assembled gold nanorod dimers with tip-to-tip alignment. *Nat Commun* **14**, 7192 (2023).
15. Paria D, Roy K, Singh HJ et al. Ultrahigh field enhancement and photoresponse in atomically separated arrays of plasmonic dimers. *Adv Mater* **27**, 1751–1758 (2015).
16. Benz F, Schmidt MK, Dreismann A et al. Single-molecule optomechanics in “picocavities”. *Science* **354**, 726–729 (2016).
17. Liu DJ, Wu TT, Zhang Q et al. Probing the in-plane near-field enhancement limit in a plasmonic particle-on-film nanocavity with surface-enhanced Raman spectroscopy of graphene. *ACS Nano* **13**, 7644–7654 (2019).
18. Hou SY, Tobing LYM, Wang XL et al. Manipulating coherent light–matter interaction: continuous transition between strong coupling and weak coupling in MoS_2 monolayer coupled with plasmonic nanocavities. *Adv Opt Mater* **7**, 1900857 (2019).
19. Xu YH, Hu HT, Chen W et al. Phononic cavity optomechanics of atomically thin crystal in plasmonic nanocavity. *ACS Nano* **16**, 12711–12719 (2022).
20. Mertens J, Eiden AL, Sigle DO et al. Controlling subnanometer gaps in plasmonic dimers using graphene. *Nano Lett* **13**, 5033–5038 (2013).
21. Tserkezis C, Esteban R, Sigle DO et al. Hybridization of plasmonic antenna and cavity modes: extreme optics of nanoparticle-on-mirror nanogaps. *Phys Rev A* **92**, 053811 (2015).
22. Baumberg JJ, Aizpurua J, Mikkelsen MH et al. Extreme nanophotonics from ultrathin metallic gaps. *Nat Mater* **18**, 668–678 (2019).
23. Sigle DO, Mertens J, Herrmann LO et al. Monitoring morphological changes in 2D monolayer semiconductors using atom-thick plasmonic nanocavities. *ACS Nano* **9**, 825–830 (2015).
24. Chen W, Zhang SP, Kang M et al. Probing the limits of plasmonic enhancement using a two-dimensional atomic crystal probe. *Light Sci Appl* **7**, 56 (2018).
25. Huh JH, Lee J, Lee S. Comparative study of plasmonic resonances between the roundest and randomly faceted Au nanoparticles-on-mirror cavities. *ACS Photonics* **5**, 413–421 (2018).
26. Ruan QF, Shao L, Shu YW et al. Growth of monodisperse gold nanospheres with diameters from 20 nm to 220 nm and their core/satellite nanostructures. *Adv Opt Mater* **2**, 65–73 (2014).
27. Liu LF, Krasavin AV, Zheng JS et al. Atomically smooth single-crystalline platform for low-loss plasmonic nanocavities. *Nano Lett* **22**, 1786–1794 (2022).
28. Han XB, Wang K, Xing XY et al. Rabi splitting in a plasmonic nanocavity coupled to a WS_2 monolayer at room temperature. *ACS Photonics* **5**, 3970–3976 (2018).

29. Huang SX, Ming T, Lin YX et al. Ultrasmall mode volumes in plasmonic cavities of nanoparticle-on-mirror structures. *Small* **12**, 5190–5199 (2016).
30. Xomalis A, Chikkaraddy R, Oksenberg E et al. Controlling optically driven atomic migration using crystal-facet control in plasmonic nanocavities. *ACS Nano* **14**, 10562–10568 (2020).
31. Cui XM, Lai YH, Ai RQ et al. Anapole states and toroidal resonances realized in simple gold nanoplate-on-mirror structures. *Adv Opt Mater* **8**, 2001173 (2020).
32. Huang H, Wang H, Li SS et al. WS_2–flake-sandwiched, Au-nanodisk-enabled high-quality Fabry−Pérot nanoresonators for photoluminescence modulation. *ACS Nano* **16**, 14874–14884 (2022).
33. Wang CY, Chen HY, Sun LY et al. Giant colloidal silver crystals for low-loss linear and nonlinear plasmonics. *Nat Commun* **6**, 7734 (2015).
34. Ramasubramaniam A. Large excitonic effects in monolayers of molybdenum and tungsten dichalcogenides. *Phys Rev B* **86**, 115409 (2012).
35. Schneider C, Glazov MM, Korn T et al. Two-dimensional semiconductors in the regime of strong light–matter coupling. *Nat Commun* **9**, 2695 (2018).
36. Liu XZ, Galfsky T, Sun Z et al. Strong light–matter coupling in two-dimensional atomic crystals. *Nat Photonics* **9**, 30–34 (2015).
37. Törmä P, Barnes WL. Strong coupling between surface plasmon polaritons and emitters: a review. *Rep Prog Phys* **78**, 013901 (2015).
38. Kleemann ME, Chikkaraddy R, Alexeev EM et al. Strong-coupling of WSe_2 in ultra-compact plasmonic nanocavities at room temperature. *Nat Commun* **8**, 1296 (2017).
39. Qin J, Chen YH, Zhang ZP et al. Revealing strong plasmon–exciton coupling between nanogap resonators and two-dimensional semiconductors at ambient conditions. *Phys Rev Lett* **124**, 063902 (2020).
40. Zheng D, Zhang SP, Deng Q et al. Manipulating coherent plasmon–exciton interaction in a single silver nanorod on monolayer WSe_2. *Nano Lett* **17**, 3809–3814 (2017).
41. Wen JX, Wang H, Wang WL et al. Room-temperature strong light–matter interaction with active control in single plasmonic nanorod coupled with two-dimensional atomic crystals. *Nano Lett* **17**, 4689–4697 (2017).
42. Liu RM, Zhou ZK, Yu YC et al. Strong light-matter interactions in single open plasmonic nanocavities at the quantum optics limit. *Phys Rev Lett* **118**, 237401 (2017).
43. Akselrod GM, Ming T, Argyropoulos C et al. Leveraging nanocavity harmonics for control of optical processes in 2D semiconductors. *Nano Lett* **15**, 3578–3584 (2015).
44. Sun JW, Hu HT, Zheng D et al. Light-emitting plexciton: exploiting plasmon–exciton interaction in the intermediate coupling regime. *ACS Nano* **12**, 10393–10402 (2018).
45. Zhu GP, Shi XQ, Huang GY et al. Highly polarized light emission of monolayer WSe_2 coupled with gap-plasmon nanocavity. *Adv Opt Mater* **10**, 2101762 (2022).
46. Li CY, Wang QF, Diao H et al. Enhanced photoluminescence of monolayer $MoSe_2$ in a double resonant plasmonic nanocavity with Fano resonance and mode matching. *Laser Photonics Rev* **16**, 2100199 (2022).
47. Zhao WJ, Wang SF, Liu B et al. Exciton–plasmon coupling and electromagnetically induced transparency in monolayer semiconductors hybridized with Ag nanoparticles. *Adv Mater* **28**, 2709–2715 (2016).
48. Li ZW, Liu CX, Rong X et al. Tailoring MoS_2 valley-polarized photoluminescence with super chiral near-field. *Adv Mater* **30**, 1801908 (2018).
49. Wen T, Zhang WD, Liu S et al. Steering valley-polarized emission of monolayer MoS_2 sandwiched in plasmonic antennas. *Sci Adv* **6**, eaao0019 (2020).
50. Sun JW, Hu HT, Pan D et al. Selectively depopulating valley-polarized excitons in monolayer MoS_2 by local chirality in single plasmonic nanocavity. *Nano Lett* **20**, 4953–4959 (2020).
51. Kim S, Lim YC, Kim RM et al. A single chiral nanoparticle induced valley polarization enhancement. *Small* **16**, 2003005 (2020).
52. Li SS, Wang H, Wang J et al. Control of light–valley interactions in 2D transition metal dichalcogenides with nanophotonic structures. *Nanoscale* **13**, 6357–6372 (2021).
53. Huang JN, Akselrod GM, Ming T et al. Tailored emission spectrum of 2D semiconductors using plasmonic nanocavities. *ACS Photonics* **5**, 552–558 (2018).
54. Park KD, Jiang T, Clark G et al. Radiative control of dark excitons at room temperature by nano-optical antenna-tip Purcell effect. *Nat Nanotechnol* **13**, 59–64 (2018).
55. Lo TW, Chen XL, Zhang ZD et al. Plasmonic nanocavity induced coupling and boost of dark excitons in monolayer WSe_2 at room temperature. *Nano Lett* **22**, 1915–1921 (2022).
56. Luo Y, Liu N, Li XZ et al. Single photon emission in WSe_2 up 160 K by quantum yield control. *2D Mater* **6**, 035017 (2019).
57. Tran TN, Kim S, White SJU et al. Enhanced emission from interlayer excitons coupled to plasmonic gap cavities. *Small* **17**, 2103994 (2021).
58. Zhou Y, Scuri G, Wild DS et al. Probing dark excitons in atomically thin semiconductors via near-field coupling to surface plasmon polaritons. *Nat Nanotechnol* **12**, 856–860 (2017).
59. Zhang XX, Cao T, Lu ZG et al. Magnetic brightening and control of dark excitons in monolayer WSe_2. *Nat Nanotechnol* **12**, 883–888 (2017).
60. Jadczak J, Glazov M, Kutrowska-Girzycka J et al. Upconversion of light into bright intravalley excitons via dark intervalley excitons in hBN-encapsulated WSe_2 monolayers. *ACS Nano* **15**, 19165–19174 (2021).
61. Qi PF, Dai YC, Luo Y et al. Giant excitonic upconverted emission from two-dimensional semiconductor in doubly resonant plasmonic nanocavity. *Light Sci Appl* **11**, 176 (2022).
62. Mueller NS, Arul R, Kang GW et al. Photoluminescence upconversion in monolayer WSe_2 activated by plasmonic cavities through resonant excitation of dark excitons. *Nat Commun* **14**, 5726 (2023).
63. Rahaman M, Zahn DRT. Plasmon-enhanced Raman spectroscopy of two-dimensional semiconductors. *J Phys Condens Matter* **34**, 333001 (2022).
64. Cong X, Liu XL, Lin ML et al. Application of Raman spectroscopy to probe fundamental properties of two-dimensional materials. *npj 2D Mater Appl* **4**, 13 (2020).
65. Chen C, Chen XL, Yu HY et al. Symmetry-controlled electron–phonon interactions in van der Waals heterostructures. *ACS Nano* **13**, 552–559 (2019).
66. Lee JU, Woo S, Park J et al. Strain-shear coupling in bilayer MoS_2. *Nat Commun* **8**, 1370 (2017).
67. Zhang SS, Huang JQ, Yu Y et al. Quantum interference directed

chiral Raman scattering in two-dimensional enantiomers. *Nat Commun* **13**, 1254 (2022).
68. Xu HX, Aizpurua J, Käll M et al. Electromagnetic contributions to single-molecule sensitivity in surface-enhanced Raman scattering. *Phys Rev E* **62**, 4318–4324 (2000).
69. Zhang YX, Chen W, Fu T et al. Simultaneous surface-enhanced resonant Raman and fluorescence spectroscopy of monolayer $MoSe_2$: determination of ultrafast decay rates in nanometer dimension. *Nano Lett* **19**, 6284–6291 (2019).
70. Chen SY, Li P, Zhang C et al. Extending plasmonic enhancement limit with blocked electron tunneling by monolayer hexagonal boron nitride. *Nano Lett* **23**, 5445–5452 (2023).
71. Chen SY, Weng SR, Xiao YH et al. Insight into the heterogeneity of longitudinal plasmonic field in a nanocavity using an intercalated two-dimensional atomic crystal probe with a ~7 Å resolution. *J Am Chem Soc* **144**, 13174–13183 (2022).
72. Wen BY, Wang JY, Shen TL et al. Manipulating the light–matter interactions in plasmonic nanocavities at 1 nm spatial resolution. *Light Sci Appl* **11**, 235 (2022).
73. Zhu WQ, Esteban R, Borisov AG et al. Quantum mechanical effects in plasmonic structures with subnanometre gaps. *Nat Commun* **7**, 11495 (2016).
74. Savage KJ, Hawkeye MM, Esteban R et al. Revealing the quantum regime in tunnelling plasmonics. *Nature* **491**, 574–577 (2012).
75. Zhang C, Li DY, Zhang GD et al. Switching plasmonic nanogaps between classical and quantum regimes with supramolecular interactions. *Sci Adv* **8**, eabj9752 (2022).
76. Wang P, Krasavin AV, Nasir ME et al. Reactive tunnel junctions in electrically driven plasmonic nanorod metamaterials. *Nat Nanotechnol* **13**, 159–164 (2018).
77. Zhang C, Hu HT, Ma CM et al. Quantum plasmonics pushes chiral sensing limit to single molecules: a paradigm for chiral biodetections. *Nat Commun* **15**, 2 (2024).
78. Shao L, Wang XM, Xu HT et al. Nanoantenna-sandwiched graphene with giant spectral tuning in the visible-to-near-infrared region. *Adv Opt Mater* **2**, 162–170 (2014).
79. Cobas E, Friedman AL, van't Erve OMJ et al. Graphene as a tunnel barrier: graphene-based magnetic tunnel junctions. *Nano Lett* **12**, 3000–3004 (2012).
80. Turunen M, Brotons-Gisbert M, Dai YY et al. Quantum photonics with layered 2D materials. *Nat Rev Phys* **4**, 219–236 (2022).
81. Koperski M, Nogajewski K, Arora A et al. Single photon emitters in exfoliated WSe_2 structures. *Nat Nanotechnol* **10**, 503–506 (2015).
82. Branny A, Kumar S, Proux R et al. Deterministic strain-induced arrays of quantum emitters in a two-dimensional semiconductor. *Nat Commun* **8**, 15053 (2017).
83. Darlington TP, Carmesin C, Florian M et al. Imaging strain-localized excitons in nanoscale bubbles of monolayer WSe_2 at room temperature. *Nat Nanotechnol* **15**, 854–860 (2020).
84. Li SS, Chui KK, Shen FH et al. Generation and detection of strain-localized excitons in WS_2 monolayer by plasmonic metal nanocrystals. *ACS Nano* **16**, 10647–10656 (2022).
85. Mendelson N, Ritika R, Kianinia M et al. Coupling spin defects in a layered material to nanoscale plasmonic cavities. *Adv Mater* **34**, 2106046 (2022).
86. Xu XH, Solanki AB, Sychev D et al. Greatly enhanced emission from spin defects in hexagonal boron nitride enabled by a low-loss plasmonic nanocavity. *Nano Lett* **23**, 25–33 (2023).
87. Parzefall M, Szabó Á, Taniguchi T et al. Light from van der Waals quantum tunneling devices. *Nat Commun* **10**, 292 (2019).
88. McKeever J, Boca A, Boozer AD et al. Experimental realization of a one-atom laser in the regime of strong coupling. *Nature* **425**, 268–271 (2003).
89. Guselnikova O, Lim H, Kim HJ et al. New trends in nanoarchitectured SERS substrates: nanospaces, 2D materials, and organic heterostructures. *Small* **18**, 2107182 (2022).
90. Lawless J, McCormack O, Pepper J et al. Spectral tuning of a nanoparticle-on-mirror system by graphene doping and gap control with nitric acid. *ACS Appl Mater Interfaces* **15**, 38901–38909 (2023).
91. Iranzo DA, Nanot S, Dias EJC et al. Probing the ultimate plasmon confinement limits with a van der Waals heterostructure. *Science* **360**, 291–295 (2018).
92. Sun Z, Gu J, Ghazaryan A et al. Optical control of room-temperature valley polaritons. *Nat Photonics* **11**, 491–496 (2017).
93. Dufferwiel S, Lyons TP, Solnyshkov DD et al. Valley-addressable polaritons in atomically thin semiconductors. *Nat Photonics* **11**, 497–501 (2017).
94. Chen YJ, Cain JD, Stanev TK et al. Valley-polarized exciton–polaritons in a monolayer semiconductor. *Nat Photonics* **11**, 431–435 (2017).
95. Qiu L, Chakraborty C, Dhara S et al. Room-temperature valley coherence in a polaritonic system. *Nat Commun* **10**, 1513 (2019).
96. Lundt N, Dusanowski Ł, Sedov E et al. Optical valley Hall effect for highly valley-coherent exciton–polaritons in an atomically thin semiconductor. *Nat Nanotechnol* **14**, 770–775 (2019).
97. Liu XZ, Yi J, Yang S et al. Nonlinear valley phonon scattering under the strong coupling regime. *Nat Mater* **20**, 1210–1215 (2021).
98. Chen H, Jiang ZH, Hu HT et al. Sub-50-ns ultrafast upconversion luminescence of a rare-earth-doped nanoparticle. *Nat Photonics* **16**, 651–657 (2022).
99. Chen YL, Zheng JP, Zhang LL et al. Inversion of the chiroptical responses of chiral gold nanoparticles with a gold film. *ACS Nano* **18**, 383–394 (2024).
100. Yang LL, Yuan Y, Fu BW et al. Revealing broken valley symmetry of quantum emitters in WSe_2 with chiral nanocavities. *Nat Commun* **14**, 4265 (2023).
101. Wang DQ, Yang AK, Wang WJ et al. Band-edge engineering for controlled multi-modal nanolasing in plasmonic superlattices. *Nat Nanotechnol* **12**, 889–894 (2017).

Acknowledgements

This work was supported by the National Natural Science Foundation of China (62205183) and the Research Grants Council of Hong Kong (ANR/RGC, Ref. No. A-CUHK404/21).

Competing interests

Jianfang Wang serves as an Editor for the Journal, no other author has reported any competing interests.